POLITECNICO DI MILANO

Dipartimento di Elettronica, Informazione e Bioingegneria

Corso di Laurea Magistrale in Biomedical Engineering

A FULLY AUTOMATIC PIPELINE FOR QUANTITATIVE SUSCEPTIBILITY MAPPING IN THE NORMAL-APPEARING WHITE MATTER IN NEURODEGENERATIVE DEMENTIA

Relatore: Prof.ssa Anna Maria BIANCHI

Correlatore: Ing. Valeria Elisa CONTARINO

Tesi di Laurea di:

Federica PELLA

921164

Anno Accademico 2019 / 2020

Ringraziamenti

Vorrei ringraziare la Prof.ssa Anna Maria Bianchi per avermi concesso l'opportunità di partecipare a questo progetto e l'Ing. Valeria Elisa Contarino per avermi guidata, incoraggiata durante questi mesi e per aver fornito un enorme contributo al mio percorso di formazione professionale.
Ringrazio l'Ing. Silvia Siggillino e l'intero reparto di Neuroradiologia del Policlinico di Milano per il prezioso apporto che hanno dato a questo progetto.
Ringrazio inoltre Irene, con la quale ho condiviso la mia esperienza a Milano, nelle sue soddisfazioni e difficoltà.

Infine, vorrei ringraziare tutte le persone che mi hanno accompagnata durante questo mio percorso di studio: Aurelia, che considero punto di riferimento nella carriera così come nella vita; la compagnia di Pasiano, con la quale sono cresciuta e che rappresenta per me una famiglia in cui potermi sempre rifugiare; gli amici del liceo, con i quali ho condiviso alcuni dei più bei momenti durante gli anni delle superiori e non solo.

Un ringraziamento speciale va alla mia famiglia: ai miei nonni, Anna, Sante, Dina e Gino, che spero di aver reso orgogliosi, e in particolare, a mamma e papà, che hanno sempre creduto in me e senza i quali ogni ostacolo durante questo percorso sarebbe sembrato insormontabile.

Dedico questo lavoro di tesi a mio fratello Luca, per il quale mi auguro di essere sempre la sorella su cui fare affidamento. Sono certa anche il tuo sarà un percorso pieno di soddisfazioni e ottimi risultati.

Abstract

Neurodegenerative dementias are disorders characterized by loss of cognitive functioning, such as thinking, remembering, and reasoning, and by impairment of behavioural abilities under particular conditions to such an extent that person's daily life activities are compromised. Worldwide, around 50 million people have dementia and there are nearly 10 million new cases every year.

The usage of neuroimaging techniques has acquired increasing importance in the detection and characterization of these disorders. Among the different imaging tools available, MRI is exploited to study the volumetric and microstructural alterations of grey matter (GM) and white matter (WM), but also to detect changes in WM that are not distinguished on conventional MRI sequences. These regions are referred as normal-appearing white matter (NAWM) and are characterized through an analysis of the susceptibility properties of the underlying tissues, which can be quantitatively assessed with an MRI technique known as Quantitative Susceptibility Mapping (QSM).

A total of 36 subjects were recruited and scanned at 3T magnetic resonance at the Neurodegenerative Diseases Unit of *Fondazione IRCCS Ca' Granda Ospedale Maggiore Policlinico*. Twenty-five of the subjects were diagnosed with neurodegenerative dementia and underwent lumbar puncture.

The patients were subdivided according to the cerebrospinal fluid (CSF) biomarkers value. This was done in accordance with the 2018 updated guidelines of the National Institute on Aging and Alzheimer's Association (NIA-AA), which defined a reproducible and objective classification, that is the AT(N) classification. The three categories of biomarkers considered are: (1) β-amyloid - Aβ deposits; (2) hyperphosphorylated tau aggregates; (3) neurodegeneration or neuronal injury, defined by the value of the total-tau protein.

A fully automatic pipeline was implemented to characterize and study the susceptibility in the subcortical NAWM through a whole-brain multi-metric approach. Processing included three main steps: *FreeSurfer* automatic segmentation of the brain; automatic segmentation of the WM lesions with the *Lesion Prediction Algorithm* (LPA) of the *Lesion Segmentation Toolbox* (LST); QSM, obtained through the *Matlab* toolbox *STI Suite*, to evaluate the WM susceptibility changes in-vivo and in a non-invasive way.

The QSM measurements extracted from the regions of interest (ROIs) were integrated with clinical information regarding the duration of the disease, CSF biomarkers and the score of the Mini-Mental State Examination (MMSE).

Among the different classifications of the subjects considered, the one based on the value of the total-tau (T-tau) protein showed the greatest amount of statistically significant comparisons. More specifically, the SD in the temporal lobe may be a predictor of the clinical group, independently from the age.

The presented thesis work lays the foundations for a larger combined QSM-CSF biomarkers study. In addition, a multi-modal study with QSM and DTI would allow to better investigate the microstructure of the NAWM in neurodegenerative dementia.

Sommario

Le demenze neurodegenerative sono disordini caratterizzati dalla perdita di funzionalità cognitiva, come pensare, ricordare e ragionare, e dalla compromissione delle abilità comportamentali in particolari condizioni a un punto tale che le attività quotidiane della persona sono compromesse. In tutto il mondo, circa 50 milioni di persone sono affette da demenza e sono quasi 10 milioni i nuovi casi ogni anno.

L'utilizzo di tecniche di neuroimaging ha acquisito un'importanza sempre maggiore nell'individuazione e caratterizzazione di questi disordini. Tra i diversi strumenti di imaging disponibili, la MRI è sfruttata per studiare le alterazioni volumetriche e microstrutturali della sostanza grigia e della sostanza bianca, ma anche per rilevare quei cambiamenti nella sostanza bianca che non sono visibili nelle sequenze convenzionali di risonanza, indicate con il termine *normal-appearing white matter* (NAWM). Questi possono essere caratterizzate tramite un'analisi delle proprietà di suscettività valutabili in-vivo con una tecnica di risonanza di *Quantitative Susceptibility Mapping* (QSM).

Un totale di 36 soggetti è stato reclutato e sottoposto a risonanza magnetica 3T presso l'unità di malattie neurodegenerative della *Fondazione IRCCS Ca' Granda Ospedale Maggiore Policlinico.* Venticinque di questi soggetti sono affetti da demenza neurodegenerativa e sono stati sottoposti a puntura lombare.

I pazienti sono stati suddivisi secondo il valore dei biomarcatori del liquido cerebrospinale (CSF). La classificazione dei pazienti è stata eseguita in conformità con le linee guida aggiornate del 2018 del *National Institute on Aging and Alzheimer's Association* (NIA-AA), che definisce una classificazione riproducibile e oggettiva chiamata AT(N). Le tre categorie di biomarcatori considerate sono: (1) depositi di beta-amiloide (Aβ); (2) aggregati di tau iperfosforilata; (3) neurodegenerazione o danno neuronale, definibile da livelli di proteina tau totale.

Una pipeline completamente automatica è stata implementata per caratterizzare e studiare la suscettività nella NAWM sottocorticale attraverso un approccio whole-brain multi-metrico. L'elaborazione ha incluso tre passaggi fondamentali: la segmentazione automatica del cervello con *FreeSurfer*; la segmentazione automatica delle lesioni della sostanza bianca con il *Lesion Prediction Algorithm* (LPA) del *Lesion Segmentation*

Toolbox (LST); la QSM, ottenuta attraverso il *Matlab* toolbox *STI Suite*, per valutare i cambiamenti di suscettività nella sostanza bianca in-vivo e in modo non invasivo.

Le misure di QSM estratte dalle regioni di interesse (ROI) sono state integrate con informazioni di tipo clinico riguardanti la durata di malattia, i biomarcatori del liquido cerebrospinale e il punteggio del *Mini-Mental State Examination* (MMSE).

Tra le diverse classificazioni dei soggetti considerate, quella basata sul valore della proteina tau totale (T-tau) ha dimostrato il maggior numero di confronti statisticamente significativi. Più precisamente, la SD del lobo temporale potrebbe rappresentare un predittore del gruppo clinico, indipendentemente dall'età.

Il lavoro di tesi presentato pone le basi per un più ampio studio combinato di QSM e biomarcatori del liquido cerebrospinale. In aggiunta, uno studio multimodale con QSM e DTI permetterebbe una migliore indagine scientifica della microstruttura della NAWM nella demenza neurodegenerativa.

Contents

Glossary

AD: Alzheimer's Disease

ANTs: Advanced Normalization Tools

APP: Amyloid Precursor Protein

Aβ: Amyloid Beta

BBB: Blood-Brain Barrier

BET: Brain Extraction Tool

CNR: Contrast-to-Noise Ratio

CNS: Central Nervous System

CSF: Cerebrospinal Fluid

DICOM: Digital Imaging and Communication in Medicine

FDG PET: Fluorodeoxyglucose Positron Emission Tomography

FLAIR: Fluid Attenuated Inversion Recovery

FTD: Frontotemporal Dementia

GM: Grey Matter

GRE: Gradient Echo

HC: Healthy Controls

IQR: Interquartile Range

LPA: Lesion Prediction Algorithm

MCI: Mild Cognitive Impairment

MMSE: Mini-Mental State Examination

MRI: Magnetic Resonance Imaging

NAWM: Normal-Appearing White Matter

ND: Neurodegenerative Dementia

NFTs: Neurofibrillary Tangles

NIA-AA: National Institute on Aging and Alzheimer’s Association

PACS: Picture Archiving and Communication System

PPA: Primary Progressive Aphasia

P-TAU: Phosphorylated tau

QSM: Quantitative Susceptibility Mapping

SD: Standard Deviation

SPGR: Spoiled Gradient Echo

SPM: Statistical Parametric Mapping

SPSS: Statistical Package for Social Science

SWI: Susceptibility Weighted Imaging

TE: Echo Time

T-TAU: Total tau

WM: White Matter

WMHs: White Matter Hyperintensities

WMLs: White Matter Lesions

List of figures

List of tables

1. Introduction

This chapter provides an overview on the main features of the neurodegenerative dementias and on the process through which the diagnosis is given.

The usage of MRI as a fundamental biomarker of the underlying neuropathological process is described with a particular attention to two techniques, which are able to study a tissue intrinsic characteristic called susceptibility. These techniques are the Susceptibility-Weighted Imaging (SWI), whose contrast is based on the tissues underlying susceptibility, and the Quantitative Susceptibility Mapping (QSM), which carries out a quantitative measure of this tissue intrinsic characteristic.

The purpose of the study is briefly described in the final paragraph.

1.1 Neurodegenerative dementias

Dementia is an "umbrella term", including disorders characterized by loss of cognitive functioning, such as thinking, remembering, and reasoning, and by impairment of behavioural abilities under particular conditions to such an extent that person's daily life activities are compromised [1].

It is one of the major causes of disability and dependency among older people and has a physical, psychological, social, and economic impact, not only on people with dementia, but also on their carers, families and society at large. Worldwide, around 50 million people have dementia and there are nearly 10 million new cases every year [2].

This word however can be referred to many different aetiologies, such as neurodegenerative, metabolic, vascular and infectious diseases. In particular, this thesis aims to analyse dementia related to neurodegenerative processes.

Each neurodegenerative disease has relatively specific characteristic clinical features [3] and it may be histologically characterized by varying degrees of neuronal loss, gliosis, usually with abnormal protein deposition. Histological features ultimately define each neurodegenerative disease [4].

Alzheimer's disease (AD) is the first cause of dementia [1]. The different kinds of dementia analysed in this thesis are: the amnesic and non-amnesic variants of AD, the frontotemporal dementia (FTD) spectrum (comprehensive of behavioural variant of FTD and of agrammatic and semantic variants of primary progressive aphasia (PPA)), mild cognitive impairment (MCI), Lewy Body dementia (LBD).

Nowadays, there is no treatment or intervention that can be used to cure dementia or to modify its course. In addition, dementia has significant social and economic consequences in terms of medical and social care costs. In 2015, the total global societal cost of dementia was estimated to be US$ 818 billion, equivalent to 1.1% of global gross domestic product (GDP). The total cost as a proportion of GDP varied from 0.2% in low- and middle-income countries to 1.4% in high-income countries [2].

For these reasons, early diagnosis, patient's stratifications and identification of pre-symptomatic individuals at higher risk of developing a type of dementia are fundamental elements in order to "prevent the preventable" [1].

The new approach used in order to detect in-vivo evidence indicative of the neuropathological process underlying the disease, includes clinical and neuropsychological

examinations, evidence coming from biochemical (such as cerebrospinal fluid (CSF) biomarkers) and imaging tools (structural imaging through MRI and functional imaging through F-fluorodeoxyglucose-positron emission tomography (FDG-PET)) [5-8].

Particularly, the role of biochemical and imaging tools in the diagnosis of these diseases is assuming more and more importance. For example, in 2018 the National Institute on Aging and Alzheimer's Association (NIA-AA) research framework updated their diagnostic criteria of AD and shifted from a clinical to a biological definition of the disease. AD was previously divided into three distinct clinical categories (cognitively unimpaired, mild cognitive impairment and dementia), while now it is viewed as a continuum which can be identified through biomarkers and neuropathological findings [5].
A biomarker is a substance, measurement or indicator of a biological state. Its usefulness in diagnosis is related to the fact that it may exist before clinical symptoms arise. It has been demonstrated, for example, that AD begins decades before the onset of clinical symptoms of dementia through the accumulation of pathological hallmarks of the disease, consisting of β-amyloid (Aβ) deposits and neurofibrillary tangles/tau proteins [9]. Accordingly, the NIA-AA grouped AD diagnostic biomarkers into three categories: β-amyloid - Aβ deposits (A), hyperphosphorylated tau aggregates (T) and neurodegeneration or neuronal injury (N). Since a syndrome is not an aetiology but rather a clinical consequence of one or more diseases [5], a biological definition of AD, different from the clinical classification based on the patient symptoms, is a logical step toward greater understanding of the mechanisms underlying its clinical expression. Disease-modifying interventions must engage biologically defined targets, and the dementia syndrome does not denote a specific biological target(s). Furthermore, the AT(N) classification is reproducible and independent from the neurologist clinical assessment and it can provide an objective and common language with which to communicate observations. Indeed, the overall objective of these NIA-AA guidelines was to create a common framework for defining and staging the disease, so that a standardized reporting of findings across the field is facilitated [5].

In addition to the evidence coming from the biochemical tools, one of the most widely used neuroimaging techniques to support the diagnosis of neurodegenerative disorders is structural magnetic resonance imaging (MRI), since it is an easy and cheap method that permits to obtain a good contrast between grey and white matter [10]. In particular, high resolution MRI (with spatial resolution of the order of millimetres) allows

to accurately quantify in-vivo the neurodegeneration of specific cortical and subcortical grey matter (GM) regions (in terms of volume loss, morphological changes and cortical thinning), and to estimate white matter (WM) structural damage [11].

For what concerns the GM, the usage of neuroimaging techniques in the study of alterations of it in dementia is object of relevant interest for the definition of premature biomarkers of the disease. In fact, as stated before, AD can be conceptualized as a progressive consequence of two pathological changes at the level of GM: extracellular amyloid plaques, which are composed of Aβ surrounded by dystrophic neuritic processes, and neurofibrillary tangles, which are intraneuronal aggregates of insoluble cytoskeletal elements, composed mainly of phosphorylated tau protein [12].

The reason why among the different diagnostic neuroimaging techniques MRI is so used, is also related to the fact that it shows the ability to have multiple types of data with just one acquisition: brain atrophy coming from structural MRI, changes in WM tracts coming from Diffusion Tensor Imaging (DTI) and quantitative measurement of tissue magnetic susceptibility coming from Quantitative Susceptibility Mapping (QSM) can be combined to provide powerful information regarding the disease onset and progression.

1.2 White matter changes in neurodegenerative dementia

Besides GM anomalies, different neuroimaging studies have observed important changes and abnormalities in WM. These alterations are called white matter lesions (WMLs) or white matter hyperintensities (WMHs) and are represented by those areas in cerebral WM that appear hyperintense on T2-weighted or fluid attenuated inversion recovery (FLAIR) MRI. The WMLs are common incidental findings on brain images of older adults [13] and they are recognizable, often in greater extents, in AD patients (along with non-Alzheimer's dementias [14]).

Clinicopathological studies [15] differentiated three categories of WMLs: punctate, periventricular, and confluent WMLs. Confluent lesions are large (usually>5mm), have irregular shape and boundaries, and look as if arising by the confluence of smaller lesions. Confluent WMLs are often attributable to small-vessel disease. Punctate lesions are small (diameter less than 5 mm), round, with a regular boundary, and tend to be multiple in the same patient. Finally, periventricular caps and halo are located in the periventricular WM adjacent to the ependymal layer.

Given these considerations, it is now important to understand how the pathological cascades occurring during the development of the disease at the level of both the cortex and WM are related one with each other and lead to the appearance of the WMHs.

First of all, the important role of vascular disease in the development of WM damage should be underlined: WMHs tend to be distributed in brain areas characterized by low perfusion levels and the density of vessels in the areas of deep, periventricular WM decreases both with normal aging and in AD [16]. Nevertheless, a recent study reported that parietal WMH pathogenesis in AD is related to axonal loss, through Wallerian-like degeneration, which corresponds to cortical phosphorylated tau burden, and demyelination in patients with AD, but to vasculopathy and ischemia in individuals without AD, leading to the idea that some WMHs are secondary to neurodegeneration in the context of AD [17].

Myelin loss and the inability of the oligodendrocytes, the cells responsible for the production and maintenance of myelin, to repair myelin damage are also two important phenomena involved in the generation of WMHs.

One of the main causes related to oligodendrocyte damage in AD is that these cells suffer from oxidative stress. In addition, other factors affecting oligodendrocytes are listed below [12].

Aβ: Several studies state that Aβ is toxic to oligodendrocytes, even if clinical trials that tried to remove the Aβ plaque in symptomatic AD patients did not prevent the progressive neurodegeneration and cognitive decline, suggesting that this toxic effect needs to be targeted earlier or it could not be the only pathology leading to cell death and atrophy.

Tau: It can affect the normal function of neurons through a toxic gain of function or a loss of its normal function in stabilizing microtubules.

Iron: During myelination, oligodendrocytes require 2–3 fold higher energy levels than other cell types in the central nervous system (CNS) to produce such an extensive amount of membrane. They synthesize cholesterol, a highly metabolically demanding process, making them vulnerable to hypoperfusion, excitotoxicity, heavy metals, and free radicals that induce oxidative stress. Oligodendrocytes have the highest iron content of all cell types and they are characterized by a low antioxidant content. For these reasons, they are one of the most vulnerable cell classes to oxidative stress in the CNS.

Hypoxia/Ischemia: Deep WM areas lie at the ends of the CNS arterial circulation and therefore they can be affected by decreases in blood flow oxygenation.

Excitotoxicity: Oligodendrocytes are vulnerable to excessive ATP and/or activation of glutamate receptors. Indeed, extensive activation of some receptors can result in their damage and, consequently, myelin destruction.

DNA damage: Age related DNA damage in myelinating oligodendrocytes may contribute to myelin loss.

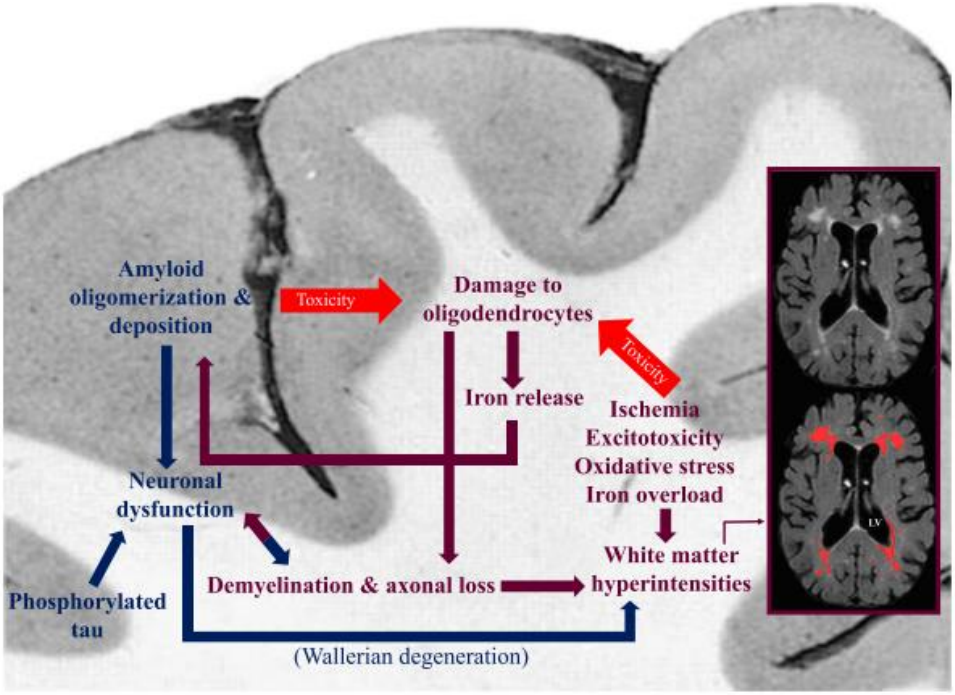

Figure 1.1 *This figure summarizes the pathological cascades, and their relation with each other, during the development of the disease in white matter and cortex. WMHs are labelled with red in the MRI (FLAIR) scan. Blue arrows: direction of the damages originating in GM. Maroon arrows: direction of the damages originating in white matter. LV: lateral ventricle levels* [12].

As previously mentioned, WMHs are implicated in the aetiology of dementia. However, it was demonstrated that WM damage spreads beyond the area of visible WMH, suggesting that the same pathogenic steps are responsible for both the lesions and the subtle "pre-visible" alterations in the surrounding normal-appearing white matter (NAWM) [38]. Thus, the term NAWM is used to refer to the regions of WM that appear normal on traditional MR imaging sequences, but that are characterized by some abnormalities.

Advanced techniques, such as DTI and QSM, can then be exploited to detect these changes. Some studies [39] demonstrated, for example, that DTI provides multiple imaging metrics, like fractional anisotropy (FA) and mean diffusivity (MD), to detect changes in WM microstructure that are not distinguished on conventional MRI. Other studies [40] showed that the myelin loss occurs in both NAWM and WMHs of cognitively impaired patients. For these reasons, and given that myelin is characterized by diamagnetic properties, QSM could be another promising tool capable of measuring the alterations occurring at the level of the NAWM.

1.3 The involvement of iron in neurodegenerative diseases

As described in the previous paragraph, iron can play an important role in the development of WMHs. Despite this, the involvement of this element in neurodegenerative dementia is not linked only to the generation of these lesions in WM. Indeed, when people age, iron deposits in different areas of the brain may directly impair normal cognitive function and behaviour. Hence, considering this fact and that age is a major risk factor associated with neurodegenerative diseases, the detection of iron, using non-invasive imaging techniques, such as Quantitative Susceptibility Mapping (QSM) via MRI, may be a useful diagnostic tool as an early indicator of disease onset [18].

Before trying to understand how the alterations of susceptibility caused by phenomena like the accumulation of iron can be measured, a brief description about how iron is implicated in these disorders from a biological point of view is presented.

1.3.1 Iron homeostasis and its role in neurological function

Iron is an essential element for a variety of biological activities including cellular metabolism, energy production, cell growth and differentiation, and gene expression. It is able to bind oxygen, contained within the haemoglobin complex, and to transport oxygen throughout the body. It is also very important for the neuronal development, synaptic plasticity, neurotransmitter processing and myelination [19]. In the brain different types of cells, like neurons, astrocytes, microglia, and oligodendrocytes, contain iron and other biometals. Particularly, astrocytes, which compose the blood-brain barrier (BBB), take up the circulating iron and redistribute it to other cells in the CNS, while oligodendrocytes exploit it as a supply for the maintenance of myelin. Moreover, iron is necessary for an optimal mitochondrial function [20], which is critical for neurons and other cells that have significant energy metabolic requirements.

Thus, iron homeostasis is of crucial importance and it is controlled by proteins and enzymes produced in the liver, like hepcidin, which modulates the process not only by controlling the iron output of cells but also the iron input, ceruloplasmin, other iron transporters (divalent metal transporter 1 (DMT1), ferroportin, transferrin) and their receptors. Iron responsive elements (IRE) and iron regulatory proteins (IRP) are instead responsible of the levels of expression of these proteins and receptors, especially in cases

of low iron levels. In addition to iron-related proteins, Amyloid Precursor Protein (APP), which is the precursor molecule whose proteolysis generates Aβ, and tau act to regulate iron [21]. APP stabilizes ferroportin to facilitate iron export in neurons [18], while tau acts as an intracellular microtubule-associated protein, which can transport the produced APP to the cell surface to promote iron output [21]. At the same time, the activity of APP has been found to be regulated by iron [22].

1.3.2 Brain iron dyshomeostasis and the pathophysiology of the disease

Given the big number of significant functions associated to iron, the maintenance of a relatively stable state related to this element is of key importance. In fact, deficiency of iron or excessive iron, or changes in the expression of proteins that regulate it, can be catastrophic to cells and tissues and are known to contribute to numerous disorders.

Even if it is still not clear whether iron accumulation is a primary or a secondary event in aging-related neuronal death and the underlying mechanisms responsible for those changes are still not fully understood, its presence drives redox reactions, inflammatory processes as well as mitochondrial dysfunction [20].

In particular, the usage of some MRI sequences allowed to confirm the co-localization of brain iron and Aβ plaques, one of the main pathological features of neurodegenerative dementia, and showed that Aβ plaques promote the development of the illness condition. This is caused by the fact that high iron levels can both promote the aggregation of Aβ peptides, increase their cytotoxicity and impact the amyloidogenic processing of APP. Besides Aβ peptides, iron can bind to tau protein, induce tau protein phosphorylation, and aggregate phosphorylated tau protein, which is the main component of neurofibrillary tangles (NFTs), another major pathological feature of diseases like AD [21].

To date, although the specific mechanism of iron involvement in the aggregation of Aβ plaques and hyperphosphorylated tau protein is not yet clear, it has been shown that iron can accelerate this process. Nevertheless, an important consideration in discussing the levels of iron is to emphasize that an increase in total brain iron is not, alone, necessary to induce oxidative stress in the brain but, rather, an imbalance in homeostasis may have a dual effect by inducing an iron-rich environment favouring oxidative stress and cell death around amyloid plaques and NFTs, whereas other brain areas may suffer from impaired neuronal function due to iron deficiency [23].

1.4 Quantitative Susceptibility Mapping

As discussed above, different studies have demonstrated that important changes in neurodegenerative diseases occur both in the GM and WM. Some of these changes are related to magnetostatic properties of the brain, which can be detected through a magnetic resonance imaging, postprocessed contrast mechanism. Quantitative Susceptibility Mapping (QSM) has the potential to monitor in-vivo iron and demyelination levels by reconstructing magnetic susceptibility sources from field perturbations. However, it is important to underline that its mathematics relies on several theoretical approximations that require regularisation strategies.

1.4.1 Magnetic susceptibility

Magnetic susceptibility (χ) is a material property that describes the ability of a substance to become magnetized in the presence of an applied magnetic field.

When matter interacts with the magnetic field, an internal magnetization is created that either opposes or augment the external field. Thus, a material which is brought inside a static magnetic field of an MRI scanner with a magnetic field intensity H, gains a magnetization (M), defined as the quantity of magnetic dipole moment per unit volume, proportional to its magnetic susceptibility (χ). The amplitude of magnetization is therefore equal to:

$$M = \chi H \tag{1.1}$$

Magnetic materials are usually divided into two main groups. Paramagnetic materials have a positive susceptibility value that leads to their magnetic moments being aligned parallel to the main magnetic field, whilst diamagnetic materials have a negative susceptibility, and their magnetic moments align anti-parallel to it. This tissue magnetization leads to the generation of a magnetic field.

Biological tissues can be either paramagnetic or diamagnetic depending on their molecular contents and microstructure. More specifically, on the atomic level, paramagnetic susceptibility is given by spins of unpaired electrons which demonstrate a higher tendency to align with an applied magnetic field, thus amplifying the field, while diamagnetic susceptibility originates from the precession of orbital electrons about the applied external

magnetic field. The precession of electrons is modelled as a circular current generating a secondly field opposing the applied one [24]. As regards the molecular level, the availability of unpaired electrons, the distribution of electron cloud within the molecule, and the competition between electron spins and induction currents will together determine the molecule's susceptibility.

As well as the molecular content, another important element determining the magnetic property is the microstructure of the tissue: the spatial arrangement of molecules and organelles within a voxel will affect the microscopic magnetic field distribution within the voxel [25].

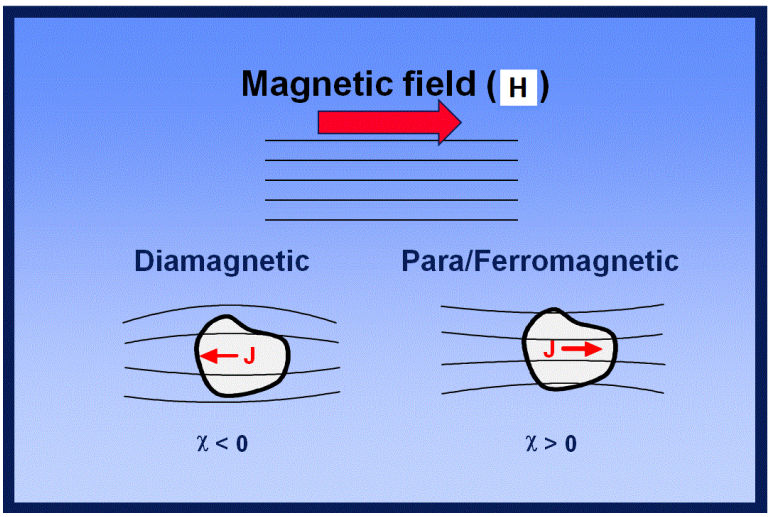

Figure 1.2 *Diamagnetic, paramagnetic and ferromagnetic materials. If the magnetization opposes the applied field, the effective field within the object is reduced, the lines are dispersed, and the effect is known as diamagnetism. If the magnetization is in the same direction as the external field, the magnetic lines are concentrated within the object, resulting in paramagnetism or ferromagnetism.*

With reference to the susceptibility properties of the brain, it has been observed that in a healthy adult brain, the most evident features of the phase and susceptibility maps are that the grey matter largely appears paramagnetic and the white matter largely diamagnetic [25]. The first one is mainly related to iron, which is ferromagnetic, while the second one is due to myelination, whose diamagnetic property is caused principally by proteins and lipids that compose it.

Accordingly, processes peculiar of neurodegenerative dementia, like iron overload and demyelination, can lead to an increase of the susceptibility, which can be detected by MRI techniques as the one which will be described in the following paragraphs.

1.4.2 Multi-echo gradient echo MRI sequence

The most commonly used sequence for visualizing the effect of magnetic susceptibility is the spoiled gradient-recalled-echo (SPGR or GRE) sequence, whose magnitude images are characterized by an exponential T_2^* decay and the phase images measure local frequency offset (f) relative to the Larmor frequency, which reflects the mean magnetic field perturbation perceived by spins within a voxel [25]. The T_2^* decay combines the effects given by the spin-spin interactions, usually characterized by the T_2 relaxation time, and the additional susceptibility and main magnetic field inhomogeneity differences, characterized by a relaxation time known as T_2'. The relation between these three terms is described by the following formula:

$$\frac{1}{T_2^*} = \frac{1}{T_2} + \frac{1}{T_2'} \tag{1.2}$$

A map of T_2^*-values could then be used to provide a quantitative measure of the amount of dephasing caused by field inhomogeneities, but this method considers only the magnitude of the MRI signal and raw MRI data is acquired as a complex-valued signal [26].
Given the fact that the phase of the signal contains important information, an MRI technique which combines both the magnitude and the phase, called Susceptibility Weighted Imaging (SWI), has been developed in order to enhance susceptibility-induced contrast.

However, the main problem with the phase of a gradient echo is that it features an artifact caused by phase wrapping (Fig. 1.3). Indeed, the GRE signal phase from MRI detects only the phase values within a range of $[-\pi,+\pi]$ and not the full phase evolution of magnetization and, since the true phase may be outside this range, aliasing may occur when it exceeds $|\pi|$ [27]. Additionally, the phase value within the brain is influenced by the phase of the receiver coils, the long-range magnetic field generated by the human body itself, and the large susceptibility difference between tissue and air. Phase brought by

sources outside a region of interest is referred to as the “background phase” and it can not only misrepresent the local tissue contrast, but also worsen the phase wrapping [25].

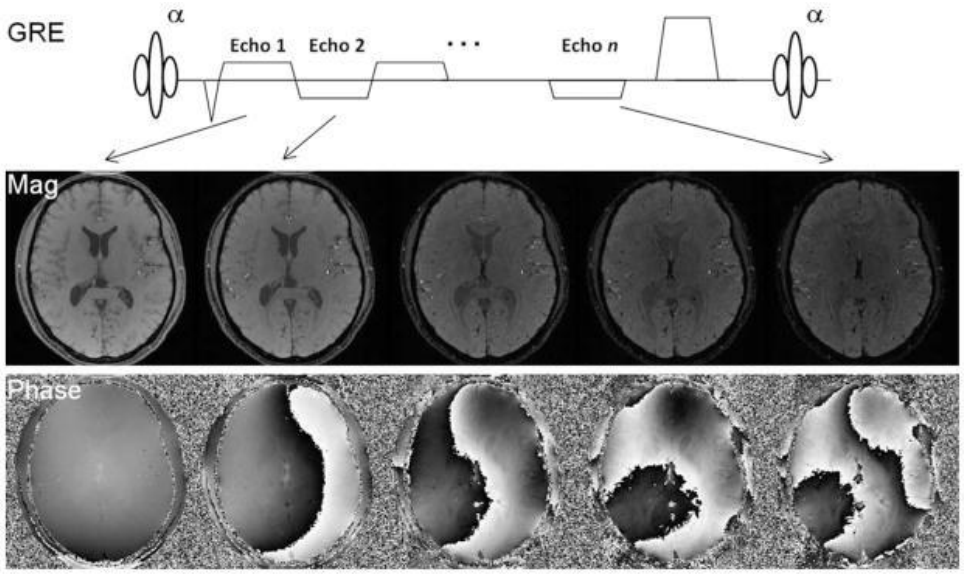

Figure 1.3 *A spoiled multi-echo gradient echo sequence [25].*

For these reasons, when creating SWI the first step that need to be applied is the phase unwrapping procedure, which is then followed by a high-pass filtering operation with the assumption that the background phase contains only low spatial frequencies [28]. After that, the filtered phase image is transformed into a special phase mask that varies in amplitude between zero and unity. This mask is multiplied a few times into the original magnitude image to create enhanced contrast between tissues with different susceptibilities [25]. The number of multiplications is chosen to optimize the contrast-to-noise ratio (CNR) in SWI and the choice is done taking into consideration the magnitude of the phase shift within the structures of interest.

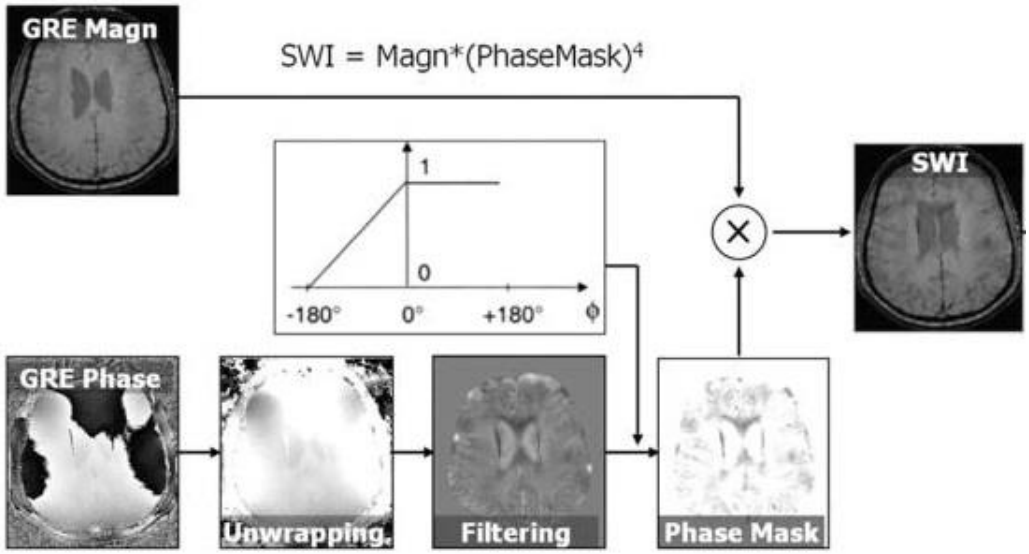

Figure 1.4 *Flowchart of the processing steps in SWI* [25].

The problem with SWI is that it depicts variations in magnetic field inhomogeneity through the signal phase, which is non-local and orientation dependent. Thus, the phase value measured in a voxel depends not only on local tissue properties, but also on the surrounding magnetic susceptibility distribution and it is not easily reproducible [25].

A solution to this is provided by QSM, that is, as well as the SWI technique, a processing based on a GRE sequence. However, QSM is able to remove these effects by directly displaying the underlying material properties, which are independent of the external field [29]. Differently from the SWI, which is generated through a processing done by the MRI machine and it is used in the clinical radiology, QSM provides a contrast that quantitatively represents the differences in susceptibility properties of the underlying tissues.

1.4.3 Quantitative Susceptibility Mapping: how is it generated?

QSM is a non-invasive MRI technique that overcomes the limitations of SWI by measuring the spatial distribution of magnetic susceptibility within an object. QSM computes the magnetic susceptibility from the phase images of GREs with the assumption that the phase shift results primarily from susceptibility-induced field inhomogeneity. The image processing steps computed by this technique and required to extract the tissue susceptibility from the phase information are described below.

As stated before, the phase values are non-local, that is the phase value measured in a voxel depends not only on local tissue properties, but also on the surrounding magnetic susceptibility distribution. This means that in a simple model where the magnetization of an imaging voxel is treated as a magnetic dipole, each dipole will produce a magnetic field (dipole field) that spatially extends beyond that voxel itself. The magnetic field at any given voxel is thus a superposition of all dipole fields generated by surrounding voxels. Because the superposition of magnetic field is linear and the field of a unit dipole is shift invariant (i.e. it does not change from one voxel to another), the relationship between the spatial distribution of susceptibility (which is proportional to magnetization) and the spatial distribution of frequency (which is proportional to magnetic field) is governed by a simple convolution. The impulse response function is the unit dipole field [25]. As a result, the field perturbation caused by a known distribution of isotropic susceptibility can be obtained by convolving the susceptibility distribution with a unit dipole kernel or by performing a pointwise multiplication in k-space [24], as described in the following formula:

$$\Delta B_z(k) = B_0(\frac{1}{3} - \frac{k_z^2}{|k^2|})\chi(\mathrm{k}) \qquad (1.3)$$

where k is the k-space vector and k_z its z-component; B_0 is the applied magnetic field, taken to be in the z-direction; $\Delta B_z(k)$ is the Fourier transform of the z-component of the magnetic field perturbation; and $\chi(k)$ is the Fourier transform of the magnetic susceptibility distribution. Finally, QSM is achieved by inverting the equation (1.3) [24].

The inversion of the equation reported above is an ill-posed problem: it becomes problematic when $k^2 = 3k_z^2$ (a conical surface in k-space, see Figure 1.5), as the coefficient becomes zero. Consequently, $\chi(k)$ cannot be accurately determined in regions near the conical surfaces. Nonetheless, a variety of approaches have been proposed to address this issue [25].

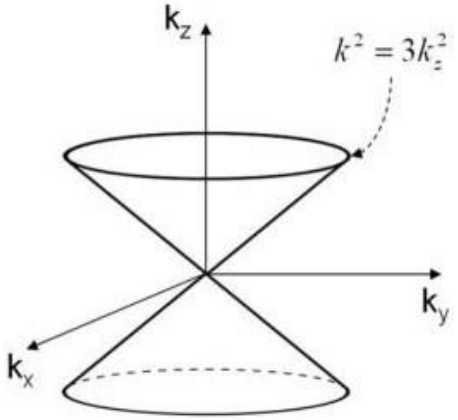

Figure 1.5 *Cone of zero coefficient. The deconvolution is an ill-posed problem because of zeros in the k-space dipole kernel on 2 conical surfaces at approximately 54.7°* [25].

Another critical factor that needs to be considered when computing QSM is related to the measurement of ΔB_z. Indeed, it must be first ensured that the phase is caused by susceptibility and not by other effects such as chemical shift, receiver coil and flow-induced phases.

Afterwards, once the susceptibility-induced phase is isolated, the data must be processed to remove phase wraps and background fields generated by sources outside the volume of interest. The process of phase unwrapping can be achieved using the conventional path-based or Laplacian-based unwrapping algorithms in spatial domain and linear fitting methods in the temporal domain [27]. Background fields can be removed using different types of algorithms, such as Projection onto Dipole Fields method (PDF), the Sophisticated Harmonic Artifact Reduction Processing (SHARP), and the method that simultaneously performs phase unwrapping and harmonic (background) phase removal using the Laplacian operator (HARPERELLA). High-pass spatial filtering can be used to simultaneously unwrap and filter the data, but this action will also remove those fields that are needed for an accurate QSM inversion.

The filtered phase in then divided by echo time (TE), so that the map of frequency variation which is obtained is referred with respect to the reference frequency of the scanner. The local field perturbation is then given by $\Delta B_z = \Delta\omega/\gamma$, where $\Delta\omega$ is the local frequency perturbation and γ is the gyromagnetic ratio [24].

At the end, the recovery of a susceptibility map from the local tissue field map is computed, taking into considerations all the issues, described above, related to the fact that

the deconvolution between the field map and the unit dipole kernel is an ill-posed problem [24].

As a convention, in a susceptibility map brighter intensities represent paramagnetic susceptibility, whereas dark intensities represent diamagnetic susceptibility [25].

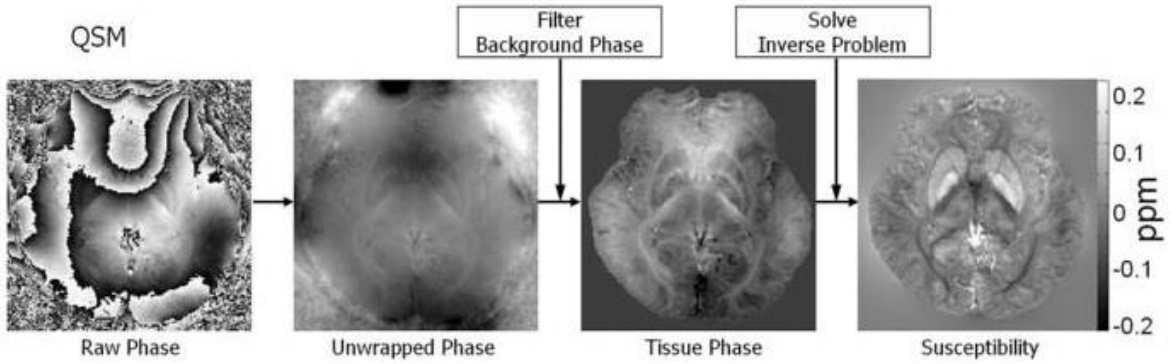

Figure 1.6 *Flowchart of the processing steps in QSM [25].*

1.5 Quantitative Susceptibility Mapping in aging and neurodegenerative dementia

A sequential increase in magnetic susceptibility values occurs in the normal aging brain due to loss of diamagnetic myelin (myelin breakdown) with iron accumulation [27]. Lots of studies have confirmed that a gradual increase in the susceptibility values happens as a normal physiological process, but this hike has a clinical application in the preclinical diagnosis of neurodegenerative diseases [27]. In the comprehensive study by Li et al. [30] the changes of regional susceptibility in the human brain in-vivo have been assessed by examining the developmental and aging process from 1 to 83 years of age. The evolution of magnetic susceptibility over this lifespan was found to display differential trajectories between the grey and the white matter. In both cortical and subcortical white matter, an initial decrease followed by a subsequent increase in magnetic susceptibility was observed, while in the grey matter, including the cortical grey matter and the iron-rich deep nuclei, magnetic susceptibility displayed a monotonic increase that can be described by an exponential growth. The trajectories in the susceptibility of white matter are consistent with the known characteristics of brain myelination during brain aging and, at the same time, the exponential growth of susceptibility contrast in grey matter is also in good agreement with the known characteristics of iron deposition.

These results suggest that susceptibility imaging may provide a promising and comprehensive tool for non-invasive assessment of myelination and iron content. In turn, an improved understanding of the spatial and temporal patterns of myelination and iron deposition during brain maturation and aging may result in better utilization of susceptibility contrast for clinical evaluations of various neurological diseases.

1.6 Project aim

The aim of the project is to develop a fully automatic pipeline for the quantification of susceptibility in the normal-appearing white matter (NAWM), in order to highlight anomalies in patients suffering from neurodegenerative dementia also in the portion of white matter that is not altered by white matter lesions.

As previously stated, some neuroimaging studies demonstrated that QSM has become a promising tool in detecting tissue changes in neurodegenerative disorders, but none of these studies have never analysed white matter that seems normal in conventional radiological assessment, that is, the NAWM.

In this work we used the unbiased classification of the patients based on the values of the CSF biomarkers.

The NAWM characterization is performed by combining the information coming from an atlas-based automatic segmentation of the WM regions and an exclusive mask of the WMLs, and the computation of statistical metrics (mean, median, SD) that accurately describe the distribution of susceptibility measures in each region.

Then, statistically analyses are carried out with the aim of testing the differences in the neuroimaging measurements among the groups and to establish a relationship among the neuroimaging measurements and the clinical variables.

2. Methods

This chapter describes the magnetic resonance data used for the study and provides an explanation of each step of the image processing pipeline that has been implemented in order to quantify susceptibility inside the NAWM.
Finally, an overview of the statistical analysis that has been carried out is given.

2.1 Subject groups

Twenty-five patients with neurodegenerative dementia (ND) were recruited at the Neurodegenerative Diseases Unit of *Fondazione IRCCS Ca' Granda Ospedale Maggiore Policlinico* as it was done in a previous study [41]. In brief, participants were referred to the centre in suspicion of dementia, and they all received - in addition to lumbar puncture - a complete neurological examination, neuropsychological assessment, and neuroimaging (brain MRI and/or FDG-PET). All the exams were performed within a 365-day interval from subjects' first visit. After the diagnostic work-up, subjects were diagnosed by expert neurologists with MCI, or dementia, according to the specific criteria of each syndrome [6,42-51].

The 25 patients are subdivided according to the values of the biomarkers extracted through the lumbar puncture. This idea is at the base of a classification, which was defined in 2018 by the NIA-AA and which has as aim that of providing a biological definition of the disease, in order to better characterize and understand the sequence of events that lead to cognitive impairment that is associated with neurodegenerative dementia [5]. However, it is important to underline that these recommendations provided by the NIA-AA should be chosen as a "research framework", not as diagnostic criteria or guidelines. Indeed, unlike the 2011 NIA-AA criteria for MCI and AD dementia based on clinical criteria (i.e. without biomarkers), the 2018 research framework is not intended for general clinical practice [5].
This scheme – which is labelled AT(N) – recognizes three general groups of biomarkers based on the nature of the pathologic process that each measures:
- biomarkers of Aβ plaques (labelled "A") are cortical amyloid PET ligand binding or low CSF Aβ42;
- biomarkers of fibrillar tau (labelled "T") are elevated CSF phosphorylated tau (P-tau) and cortical tau PET ligand binding;
- biomarkers of neurodegeneration or neuronal injury (labelled "N") are CSF T-tau, FDG PET hypometabolism, and atrophy on MR.
A cut point denoting normal (-) versus abnormal (+) values was defined for each biomarker as follows. Regarding the biomarker of Aβ plaques, a value of CSF Aβ42 lower than 640 pg/mL (598-674, 95% Cl) was considered as abnormal; for the biomarker of fibrillar tau a value of CSF P-tau greater than 580 pg/mL (540-610, 95% Cl) was identified as abnormal

and, for the biomarker of neurodegeneration, a value of CSF T-tau greater than 61 pg/mL was denoted as abnormal.

To sum up, we used the label "A+" to refer to subjects with neurodegenerative dementia having an abnormal value of the biomarker of Aβ plaques; the label "A-" to refer to subjects with neurodegenerative dementia having a normal value of the biomarker of Aβ plaques; the label "T+" to refer to subjects with neurodegenerative dementia having an abnormal value of the biomarker of fibrillar tau; the label "T-" to refer to subjects with neurodegenerative dementia having a normal value of the biomarker of fibrillar tau; the label "N+" to refer to subjects with neurodegenerative dementia having an abnormal value of the biomarker of neurodegeneration; the label "N-" to refer to subjects with neurodegenerative dementia having a normal value of the biomarker of neurodegeneration.

Beside the ND group, 11 *Healthy Controls* (HC) were recruited. These are subjects without cognitive deficits recruited from non-consanguineous relatives of the patients.

Demographic data are summarized in Table 2.1. Clinical data describing the scores of the neuropsychological test Mini-Mental State Examination (MMSE) and the duration of the disease are reported in Table 2.2.

Group	**Number of subjects**	**Age (median±IQR)**	**Age Range**	**M/F**
ND	25	70,00 ± 8,00	60 - 81	17/8
A+	14	70,00 ± 3,75	61 - 79	8/6
A-	11	69,00 ± 10,50	60 - 81	9/2
T+	12	72,50 ± 4,25	63 - 79	8/4
T-	13	67,00 ± 7,00	60 - 81	9/4
N+	10	73,00 ± 3,50	69 - 79	7/3
N-	15	67,00 ± 7,00	60 - 81	10/5
HC	11	64,00 ± 17,50	51 - 80	9/2

Table 2.1 *Group demographic data.*

Group	Duration disease (median±IQR)	MMSE (median±IQR)	MMSE Range
ND	3,00 ± 3,00	23,0 ± 8,0	4 - 29
A+	3,00 ± 4,00	22,5 ± 6,0	4 - 29
A-	3,00 ± 3,00	27,0 ± 6,0	7 - 29
T+	3,50 ± 4,00	19,5 ± 9,0	7 - 29
T-	3,00 ± 3,00	26,0 ± 5,0	4 - 29
N+	4,00 ± 5,00	19,5 ± 7,0	7 - 28
N-	3,00 ± 3,00	26,0 ± 5,0	4 - 29
HC	/	30,0 ± 1,0	20 - 30

Table 2.2 *Group clinical data.*

2.1.1 CSF biomarkers determination

CSF levels of amyloid beta (Aβ), phosphorylated-tau (P-tau) and total-tau (T-tau) were measured using Innotest ELISAs following manufacturer's instructions (Fujirebio, Ghent, Belgium).

2.2 Image acquisition

Whole brain images were acquired in a 3T Philips Achieva d-Stream scanner. In this thesis three different sequences were used during the processing, whose parameters are reported here:

- 3D T1-weighted images: Repetition time = 10,46ms; Echo time = 4,93ms; Pixel spacing = 0,67mm; Slice thickness = 0,70mm; Spacing between slices = 0,70mm; Flip angle = 8°; Rows = 384; Columns= 384.
- 3D FLAIR images: Repetition time = 4800ms; Echo time = 321,93ms; Pixel spacing = 0,52mm; Slice thickness = 1,00mm; Spacing between slices = 0,50mm; Flip angle = 90°; Rows = 480; Columns= 480.
- Multi-echo GRE sequence: Repetition time = 51,00ms; Number of echoes = 6; Echo time = 9,80ms-17,00ms-23,00ms-30,00ms-37,00ms-44,00ms; Pixel spacing = 0,45mm; Slice thickness = 2,00mm; Spacing between slices = 1,00mm; Flip angle = 20°; Rows = 512; Columns = 512.

MR images were clinically evaluated and processed at Neuroradiology Unit, *Fondazione IRCCS Ca' Granda Ospedale Maggiore Policlinico*.

2.3 Image processing pipeline

In Figure 2.1 the fully automatic pipeline implemented to process the images is shown; each step will be better described in the following paragraphs.

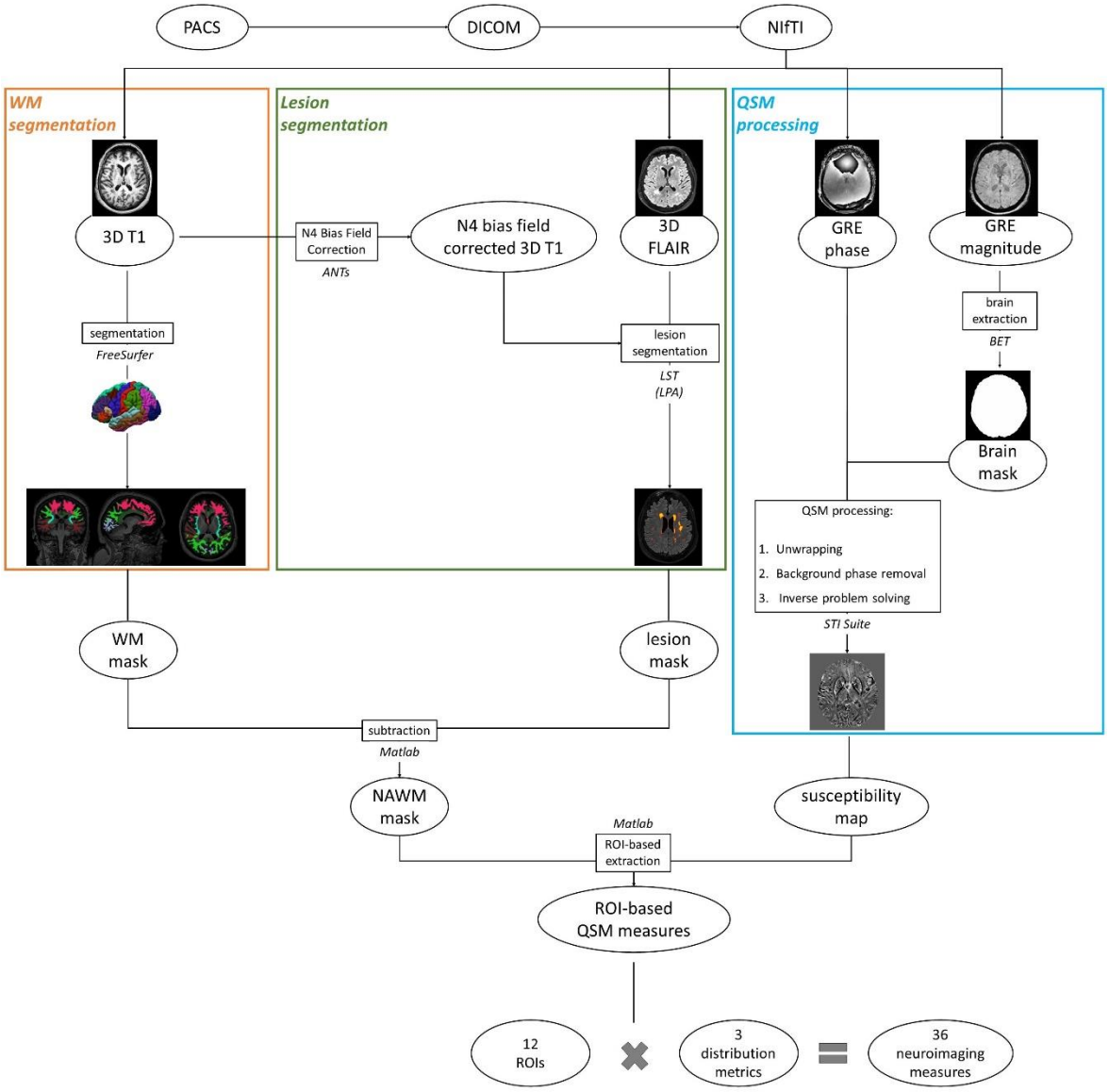

Figure 2.1 *Image processing pipeline.*

2.3.1 Pre-processing

3D T1-weighted, 3D FLAIR and GRE images were used as inputs in the image processing pipeline.

In the first place, images stored in *Digital Imaging and Communication in Medicine* (DICOM) format were retrieved from the *Picture Archiving and Communication System* (PACS) of the hospital. Once downloaded, the images were converted into NIfTI format using *dcm2niix* function in the software *MRIcroGL*. Indeed, DICOM format is not typically used in neuroimage processing due to the excessive dimension.

The images that were employed in the processing pipeline are shown in Figure 2.2 and Figure 2.3.

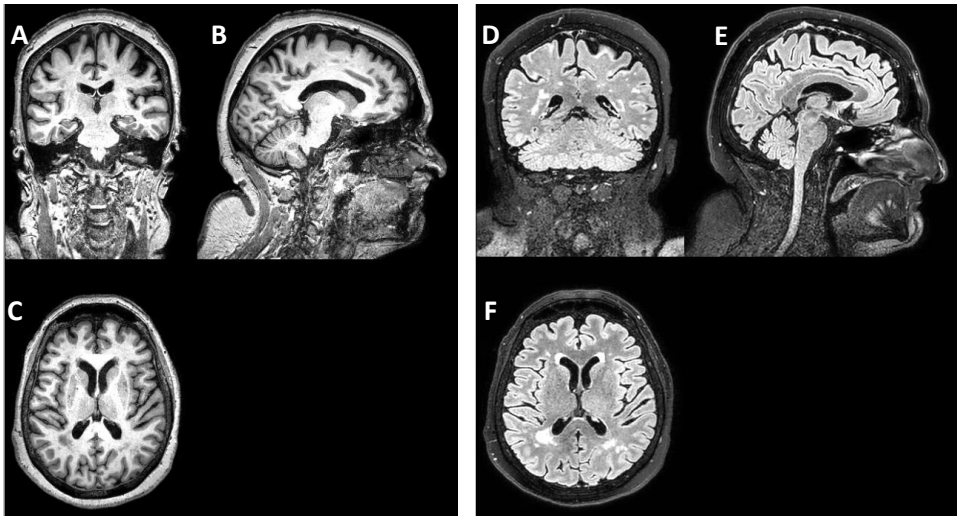

Figure 2.2 *Coronal, sagittal, axial 3DT1 (A-C) and FLAIR (D-F).*

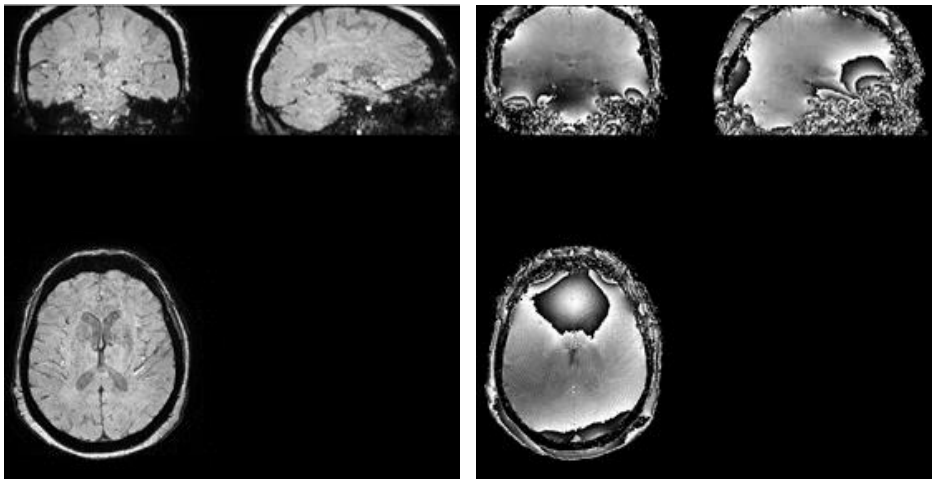

Figure 2.3 *Magnitude (left) and phase (right) of a single echo of the multi-echo GRE sequence.*

2.3.2 Subcortical WM segmentation

The automatic segmentation of the subcortical white matter in the 3D T1-weighted images was obtained using the open source software *FreeSurfer* [35], whose segmentation is based on the Desikan-Killiany atlas [36,37]. The function *recon-all*, implemented in this software, requires as input the subject data upon which to operate, and generates as output a brain image with different labels. The indexes of the labels allow the identification of each brain structure for each hemisphere. The brain labelling begins at the cortical level and then, starting from this cortical parcellation, continues with the subsequent subcortical white matter segmentation.

Figure 2.4 represents an example of labelled subcortical white matter, subdivided into the 6 lobes considered in this work (frontal, cingulate, occipital, temporal, parietal, insula), superimposed to a 3D T1-weighted image.

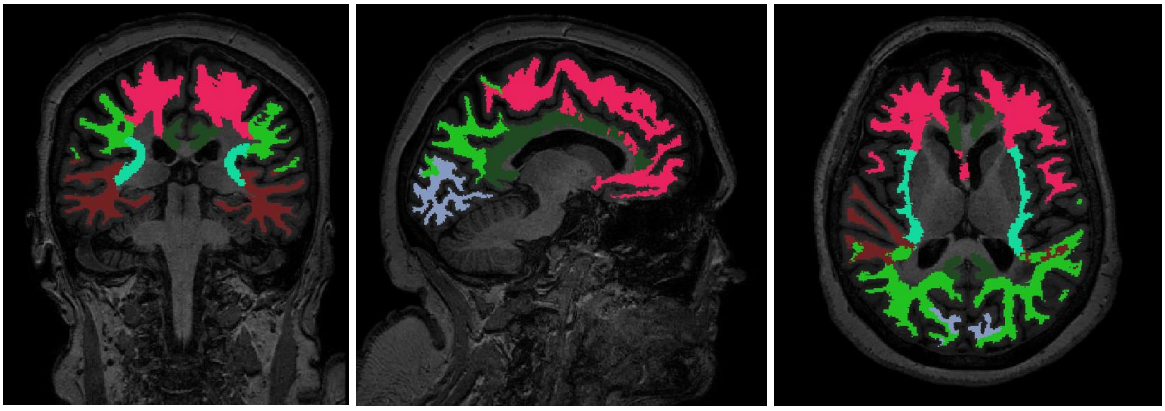

Figure 2.4 *Segmented subcortical WM superimposed on a 3D T1-weigthed image.*

2.3.3 Lesion segmentation

In order to characterize the susceptibility of the NAWM, a segmentation of the WMLs was necessary to create the mask. The WMLs were segmented by using the *lesion prediction algorithm* (LPA) [31] as implemented in the LST toolbox version 3.0.0 for *Matlab*'s *Statistical Parametric Mapping* (SPM) 12.

This algorithm consists of a binary classifier in the form of a logistic regression model, which has been trained on the data of 53 multiple sclerosis patients with severe lesion patterns. However, given the common processes that undergo both this disease and neurodegenerative diseases regarding the white matter lesions, we chose to apply this

algorithm also to the group of study of this work. Nevertheless, before proceeding with the processing, the results of the lesion segmentation were assessed by an expert neuroradiologist.

The LPA requires as input a FLAIR image and additional images are possible, as a reference image during a coregistration step (before the main lesion segmentation). As additional image we used the 3D T1-weighted image.

The algorithm corrects the FLAIR image for low-frequency intensity non-uniformity known as *bias field* and it extracts two features from the available MR images. The first feature is the position of each brain voxel in a standard space (MNI, *Montreal National Institute*). To this end, FLAIR images which have been coregistered to the T1-weighted images are normalized to MNI space using the *Normalize* function implemented in SPM. This creates an inverse deformation field which can be used to map MNI coordinates into the subject specific native space [31]. The second feature extracted is the so-called lesion belief map. This image is produced by the following steps. First, the FLAIR image is roughly segmented into the three main tissue classes GM, WM, and CSF. Subsequently, FLAIR intensities are standardized by dividing each voxel by the mean of segmented GM and the mean of standardized GM voxels is also subtracted from all FLAIR intensities. After this step only positive differences are kept, negative values are set to zero. Furthermore, the remaining differences are multiplied by a tissue probability map for WM, which is obtained by applying the inverse deformation field described before to the tissue probability maps included in SPM [31]. The resulting lesion belief map shows voxels that appear hyperintense in the FLAIR image and which are likely to be part of WM in healthy subjects, thus, possible lesion candidates.

In the end, the outputs produced by the algorithm are the bias corrected coregistered FLAIR image and the lesion probability map, in which each voxel can assume a value between 0 and 1 according to its probability of representing a lesion voxel. It is also relevant to mention that we decided to perform a bias field correction also in the 3D T1-weighted images given as reference input to the algorithm. Such correction was done by using *N4BiasFieldCorrection* function implemented in the open source tool *Advanced Normalization Tools* (ANTs).

Figure 2.5 shows an example of automatic segmentation of lesions performed by the LPA algorithm for SPM12.

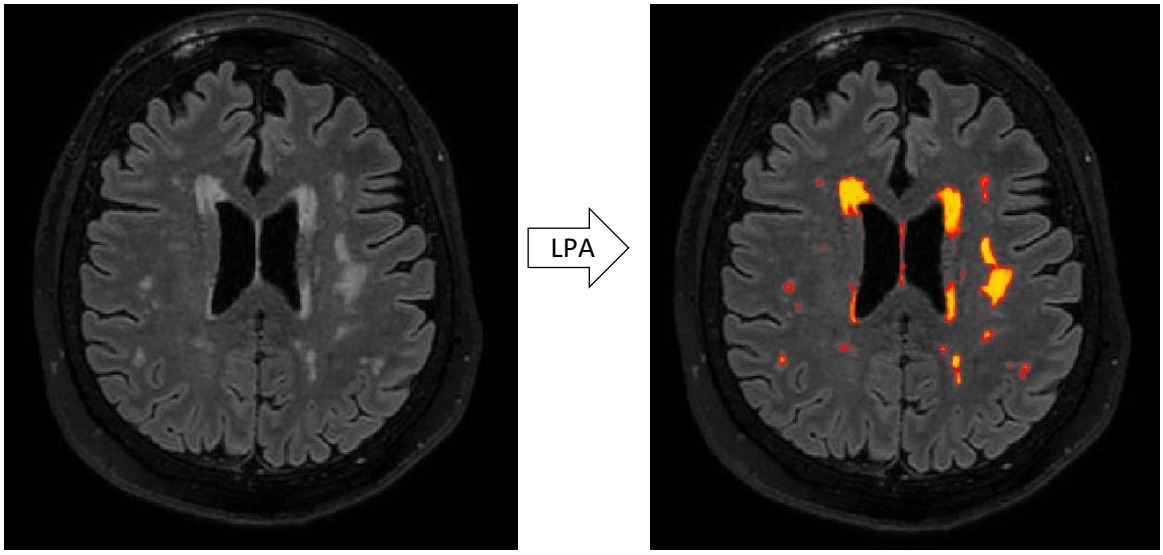

Figure 2.5 *Automatic segmentation of WMLs using the LPA algorithm.*

2.3.4 Normal-appearing white matter segmentation

Since the aim of this work is to study and analyse quantitatively the alterations of susceptibility in the NAWM, it was necessary to create, first of all, a mask representing the NAWM. In other words, a volume containing 1s in correspondence of a NAWM voxel, 0s in correspondence of WMLs and other structures. In order to create it, the WMLs mask, obtained with the LPA, was subtracted from the subcortical WM mask, processed with *FreeSurfer*. This operation was computed using *Matlab* and it was possible because the two masks were in the same anatomical space. Indeed, the mask of the lesions was obtained from the FLAIR image, which was automatically coregistered to the 3D T1-weighted image by the LPA algorithm and, at the same time, the subcortical WM segmentation used as input the 3D T1-weighted image.

2.3.5 QSM data processing

The susceptibility maps were computed from a *Matlab*-based toolbox, named *STI Suite*. The toolbox includes implementations of methods for phase processing and QSM. These methods offer excellent robustness and can produce local tissue phase free of erroneous phase discontinuities [32].

First of all, the GRE images in DICOM format were read with the *Read_DICOM_HW* function, and then separated into magnitude and phase [32]. The

resulting magnitude images were used to obtain the mask of the brain tissue employing the *Brain Extraction Tool* (BET) in FSL, a comprehensive library of analysis tools for MRI brain imaging data.

Secondly, a Laplacian-based approach to achieve efficient 3D phase unwrapping was applied using the *MRPhaseUnwrap* formula provided by the toolbox. Figure 2.6 represents an example of the unwrapped phase obtained.

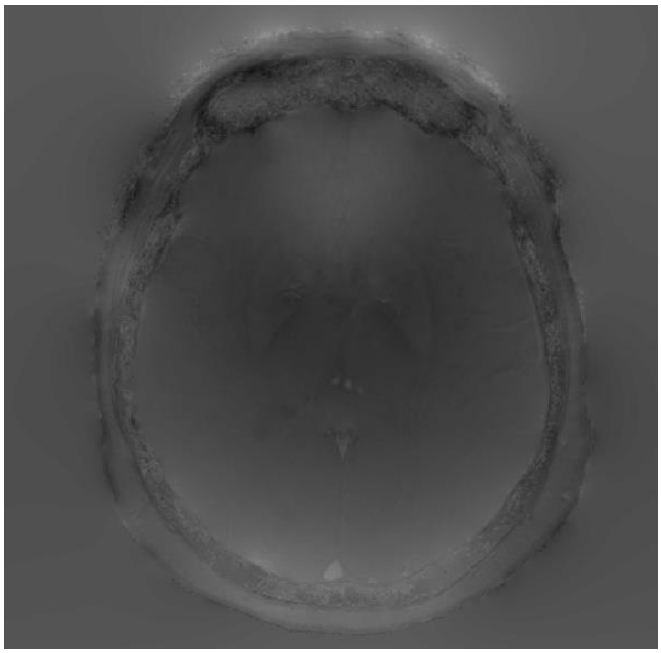

Figure 2.6 *Unwrapped phase of one echo.*

After that, the background phase was removed using *V_SHARP* function, which uses a varying spherical kernel to remove the background phase and preserve the contrast near the boundary of the brain. The amplitude of devolution kernel can be changed acting on the *smvsize* parameter of the function, which varies the radius of the spherical kernel. The power of this devolution kernel is pretty large for small *smv* radius, but it drops off rapidly with increasing *smv* radius. As a result, using a sphere filter with a small diameter may cause large amplification of the residual phase error; on the other hand, using a larger diameter can lead to a much lower level of phase error, but, at the same time, there would be larger regions at the boundary to be discarded [33]. After several tries, we empirically decided to use a quite small value (4 mm), because this was the best compromise for our

images. An example of the tissue phase, which was got as output of the *V_SHARP* function, is represented in Figure 2.7.

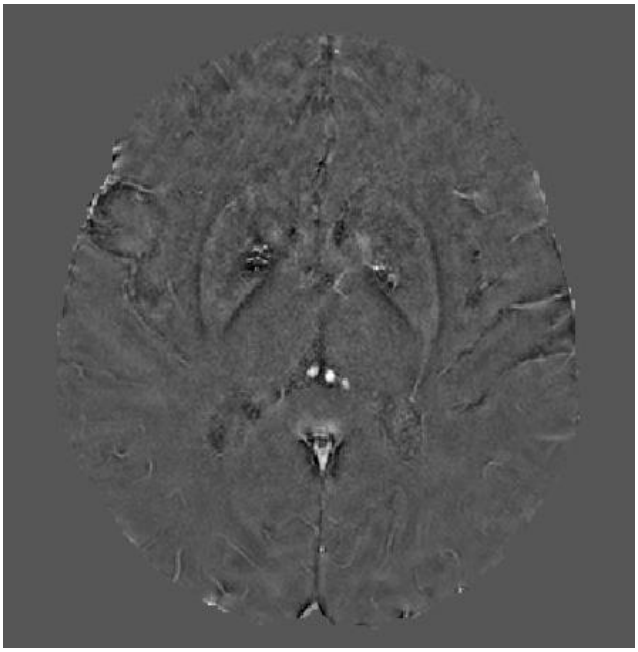

Figure 2.7 *Tissue phase of one echo.*

In the last step, the susceptibility maps were computed using the function *QSM_star,* which is able to solve the ill-posed inverse problem, that is, the final step for obtaining the maps, given as input the mean of the 6 echoes tissue phase. This function is based on a two-level reconstruction algorithm (STAR-QSM), that was developed by tuning a regularization parameter to automatically reconstruct both large and small susceptibility values [34]. First, an estimation of only the strong susceptibility sources is calculated; then the dipole field associated to these strong susceptibility sources is determined and subtracted from the total phase; finally, the susceptibility map from the residual phase, that corresponds to weaker sources, is calculated and superimposed to the map of the stronger sources [34]. As stated in [34], STAR algorithm presents a better performance in the reduction of streaking artefacts and from a computational point of view, with respect to other methods, like sparse linear equation and least squares (ILSQR).
A susceptibility map computed with this processing is pictured in Figure 2.8.

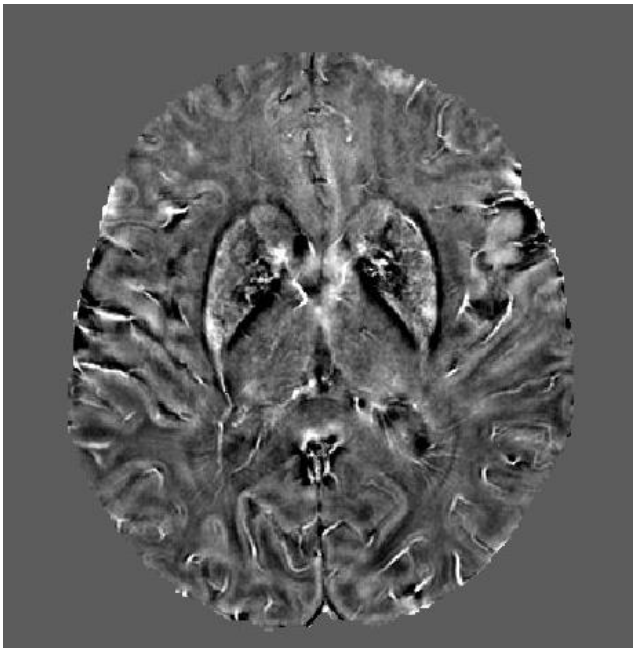

Figure 2.8 *Susceptibility map obtained with STAR-QSM.*

2.3.6 Coregistration between QSM and FreeSurfer segmentation

A coregistration procedure was computed in order to overlap the susceptibility maps and the images containing the segmented subcortical WM (as described in paragraph 2.3.2). Since the susceptibility maps were obtained from the GRE sequence, whereas *FreeSurfer* segmentation worked on 3D T1 images, the coregistration was needed to reduce overlap discrepancies between the two images, that may be caused by small movements of the patients between the acquisition of the two sequences. More specifically, this was performed by setting the 3D T1 image as reference image, the magnitude derived from the GRE sequence as source image and the susceptibility map as other image.
Interpolation was kept to the default setting, which is trilinear interpolation.

2.3.7 Neuroimaging measurements

Once the susceptibility maps were obtained, a ROI-based extraction was exploited in *Matlab*.
After the coregistration steps above described, all the images (the susceptibility map and the NAWM segmentation) were precisely overlapped each other. Thus, the mask of the

NAWM subdivided into the 6 lobes was used as ROIs and it was possible to calculate QSM measurements inside each ROI.

The QSM measures consist of mean, median and SD of QSM values in the 12 ROIs (6 lobes in each hemisphere of the subcortical WM: frontal, cingulate, occipital, temporal, parietal, insula).

2.4 Statistical analysis

Statistical Package for Social Science (*IBM SPSS statistics,* version 26.0.0.0) and *Matlab* (version 2019b) were used to analyse the data.

During this phase of the work we decided to make different statistical analyses considering, first, a subdivision of the subjects that simply differentiates between ND and HC groups, and then, three different classifications based on the value of the CSF Aβ42 (A+, A-, HC), CSF P-tau (T+, T-, HC) and CSF T-tau (N+, N-, HC), respectively.

In summary, the different classifications that are considered in this thesis subdivide the subjects in the following ways:

1. ND group, HC
2. Abnormal value of CSF Aβ42 (A+), normal value of CSF Aβ42 (A-), HC
3. Abnormal value of CSF P-tau (T+), normal value of CSF P-tau (T-), HC
4. Abnormal value of CSF T-tau (N+), normal value of CSF T-tau (N-), HC.

Since the number of samples of our group of study is limited, we decided to implement a non-parametric approach. The statistical significance was set to 0.05.

2.4.1 Demographic data (age and sex) group comparisons

Mann-Whitney U test was used to compare age between ND and HC, while Kruskal-Wallis H test (rank-based non-parametric test) was used to test differences among CSF biomarkers-defined patient subgroups and HC.

Pearson's chi-square test was employed to compare sex among the two groups of classification number 1 (see Paragraph 2.4) and among the three groups of classifications number 2, 3 and 4.

2.4.2 Clinical data (disease duration and MMSE's score) group comparisons

Three Mann-Whitney U tests were used to test differences on disease duration (measured in years) between A+ and A-, between T+ and T-, and between N+ and N-.

Then, one Mann-Whitney U test was used to compare MMSE's scores among the two clinical groups of classification number 1 and three Kruskal-Wallis H tests were used to compare MMSE's scores among the three clinical groups of classifications number 2, 3

and 4. When Kruskal-Wallis test reached statistical significance, multiple comparisons between groups were analysed.

2.4.3 Neuroimaging measurements analysis

Mann-Whitney U test was used to compare mean, median and SD of the susceptibility values among the two groups considered in classification number 1, mentioned in paragraph 2.4.

Kruskal-Wallis H test was instead performed to test the differences in mean, median and SD of the susceptibility measures among the three clinical groups considered in the three classifications (classification number 2, 3 and 4 mentioned in paragraph 2.4).
When Kruskal-Wallis test reached statistical significance, multiple comparisons between groups were performed with post hoc test in order to define where the differences occurred between the groups.

For those groups between which there was a significant difference in the post hoc test, a correction for age and a binomial logistic test were performed.
The correction for age was made by means of the Quade's test, a "non-parametric ANCOVA". In order to produce this analysis in SPSS the required steps are the following:

1) Rank the dependent variable (neuroimaging measurement which reached a statistical significance in the post hoc test) and any covariate (age). This is done for all cases, ignoring the grouping variable.
2) Run a linear regression of the ranks of the dependent variable on the ranks of the covariates, saving the residuals. Again, the grouping factor is still ignored.
3) Run a one-way analysis of variance (ANOVA), using the residuals from the regression in the prior step as the dependent variable, and the grouping variable as the factor. The F-test resulting from this ANOVA is the F-statistic Quade used.

The binomial logistic regression is made to predict the probability that an observation falls into one of the two categories of a dichotomous dependent variable based on one or more independent variables. In our case the dependent variable is the one which describes the belonging of a subject to one of the two groups of the classification 2, 3 and 4, while the independent variables were one at a time of the neuroimaging measurement that reached statistical significance in the post hoc test and the age.

2.4.4 Neuroimaging measurements and clinical variables correlation

Spearman's correlation tests were performed between each neuroimaging measurement and each of the following clinical variables: disease duration, MMSE's score, Aβ, P-tau and T-tau.

3. Results

In this chapter, the results of the statistical analyses are reported as follows: group differences in age, sex, disease duration and MMSE's score; group differences in neuroimaging measurements and relative correction for age; correlation between neuroimaging measurements and clinical variables.

The groups are first considered as neurodegenerative dementia and healthy controls, and then the neurodegenerative dementia group is further subdivided according to the CSF biomarkers.

3.1 Demographic and clinical data differences among groups

3.1.1 Age differences among groups

Age did not statistically differ among groups neither considering classification number 1 mentioned in paragraph 2.4 (U = 103.0, p = .247), nor considering classifications number 2 ($\chi^2(2) = 1.408$, p = .495), 3 ($\chi^2(2) = 4.128$, p = .127) and 4 ($\chi^2(2) = 5.653$, p = .059).

It is important to underline that the significance value in the latter classification might highlight a trend.

3.1.2 Sex differences among groups

Sex did not statistically differ among the groups neither considering classification number 1 ($\chi^2(1) = .727$, p = .394), nor considering classification number 2 ($\chi^2(2) = 2.597$, p = .273), 3 ($\chi^2(2) = .747$, p = .688) and 4 ($\chi^2(2) = .760$, p = .684).

3.1.3 Disease duration differences among groups

Disease duration (measured in years) did not statistically differ among groups as determined by Mann-Whitney U test.

As regards the disease duration, the differences among groups were tested only for classifications number 2, 3 and 4, mentioned in paragraph 2.4, and not for classification number 1, given that this subdivision describes only two clinical groups and one of them is the HC group, for which disease duration variable is not defined.

Disease duration did not statistically differ in any of the three classifications considered: classification number 2 (U = 76.5, p = .979), 3 (U = 60.0, p = .347) and 4 (U = 57.0, p = .338).

3.1.4 MMSE's score differences among groups

MMSE's score statistically differed among the groups both considering classification number 1 (U = 251.0, p = .000), and classification number 2 ($\chi^2(2) = 16.645$, p = .000), 3 ($\chi^2(2) = 17.364$, p = .000), 4 ($\chi^2(2) = 17.804$, p = .000).

Post hoc tests showed a statistically significant difference between A+ and HC (p = .000) and between A- and HC (p = .006) considering classification number 2; between T+ and HC (p = .000) and between T- and HC (p = .005) considering classification number 3; between N+ and HC (p = .000) and between N- and HC (p = .003) considering classification number 4.

3.2 Neuroimaging measurements in neurodegenerative dementias

In the following paragraphs the results of the statistical tests on the neuroimaging measurements are reported for classifications described in 2.4. The results of the post hoc tests and the following correction for the "age" variable are presented.

3.2.1 Neuroimaging measurements group comparison (classification: ND group, HC)

The results of the Mann-Whitney test run to compare mean, median and SD of the susceptibility measures among the two groups (ND vs HC) are reported in Table 3.1.

ROI	mean		median		SD	
	lh	rh	lh	rh	lh	rh
wm-frontal-lobe	0,542	0,735	0,276	0,172	0,710	0,183
wm-cingulate-lobe	0,520	0,813	0,396	1,000	0,542	0,839
wm-occipital-lobe	0,919	0,565	0,919	0,787	0,542	0,685
wm-temporal-lobe	0,735	0,276	0,565	0,919	0,161	0,008
wm-parietal-lobe	0,735	0,839	0,919	0,735	0,565	0,866
wm-insula-lobe	0,542	0,919	0,612	0,919	0,233	0,946

Table 3.1 *Mann-Whitney test on neuroimaging measurements among the two groups (ND vs HC). Red highlights significance at the 0.01 level.*

3.2.2 Neuroimaging measurements group comparison based on the biomarker of Aβ plaques - A

The results of the Kruskal-Wallis test run to compare mean, median and SD of the susceptibility measures among the three groups (A+, A- and HC) are reported in Table 3.2.

ROI	A					
	mean		median		SD	
	lh	rh	lh	rh	lh	rh
wm-frontal-lobe	0,667	0,937	0,305	0,289	0,809	0,370
wm-cingulate-lobe	0,507	0,759	0,561	0,640	0,505	0,924
wm-occipital-lobe	0,652	0,679	0,742	0,957	0,530	0,888
wm-temporal-lobe	0,681	0,398	0,767	0,804	0,359	0,026
wm-parietal-lobe	0,676	0,802	0,673	0,793	0,826	0,597
wm-insula-lobe	0,473	0,992	0,814	0,975	0,421	0,918

Table 3.2 *Kruskal-Wallis test on neuroimaging measurements among the three groups (A+, A-, HC). Yellow highlights significance at the 0.05 level.*

3.2.3 Post hoc test on neuroimaging measurements (classification A based on the biomarker of Aβ plaques)

Post hoc test showed a statistically signficant difference comparing the SD of QSM values in the right temporal lobe NAWM between A+ and HC (p = .023). The group A+ showed an increased value with respect to the group HC.

3.2.3.1 Post hoc test correction for the age

For those variables which reached statistical significance in the post hoc test (A+ and HC), a non-parametric ANCOVA was applied using a Quade's test.
The group A+ showed a statistically significant increase with respect to the group HC in the SD of QSM values in the right temporal lobe NAWM (p = .010).

3.2.3.2 Binomial logistic regression

In addition to the approach explained in the previous paragraph, for those variables which reached statistical significance in the post hoc test, a binomial logistic regression was performed to predict the probability that a subject belongs to the group A+ or HC.
The model showed that the SD of QSM values in the right temporal lobe NAWM is statistically significant in predicting the belonging of a subject to one of the two groups (p = .022), while the age is not (p = .115).

3.2.4 Neuroimaging measurements group comparison based on the biomarker of fibrillar tau - T

The results of the Kruskal-Wallis test run to compare mean, median and SD of the susceptibility measures among the three groups (T+, T- and HC) are reported in Table 3.3.

ROI	T					
	mean		median		SD	
	lh	rh	lh	rh	lh	rh
wm-frontal-lobe	0,661	0,742	0,471	0,146	0,158	0,025
wm-cingulate-lobe	0,788	0,939	0,668	0,990	0,677	0,959
wm-occipital-lobe	0,900	0,760	0,751	0,893	0,485	0,871
wm-temporal-lobe	0,920	0,521	0,770	0,992	0,332	0,034
wm-parietal-lobe	0,278	0,196	0,438	0,262	0,744	0,919
wm-insula-lobe	0,156	0,970	0,623	0,919	0,324	0,972

Table 3.3 *Kruskal-Wallis test on neuroimaging measurements among the three groups (T+, T-, HC). Yellow highlights significance at the 0.05 level.*

3.2.5 Post hoc test on neuroimaging measurements (classification T based on the biomarker of fibrillar tau)

Post hoc test showed no statistically significant differences comparing the SD of QSM values in the right frontal lobe NAWM and in the right temporal lobe NAWM in the multiple comparisons among the groups.

3.2.6 Neuroimaging measurements group comparison based on the biomarker of neurodegeneration - N

The results of the Kruskal-Wallis test run to compare mean, median and SD of the susceptibility measures among the three groups (N+, N- and HC) are reported in Table 3.4.

ROI	N					
	mean		median		SD	
	lh	rh	lh	rh	lh	rh
wm-frontal-lobe	0,739	0,481	0,517	0,045	0,338	0,017
wm-cingulate-lobe	0,570	0,406	0,551	0,758	0,741	0,731
wm-occipital-lobe	0,588	0,333	0,565	0,869	0,503	0,753
wm-temporal-lobe	0,891	0,481	0,637	0,607	0,279	0,031
wm-parietal-lobe	0,032	0,015	0,077	0,021	0,805	0,745
wm-insula-lobe	0,121	0,983	0,539	0,971	0,371	0,878

Table 3.4 *Kruskal-Wallis test on neuroimaging measurements among the three groups (N+, N-, HC). Yellow highlights significance at the 0.05 level.*

3.2.7 Post hoc test on neuroimaging measurements (classification N based on the biomarker of neurodegeneration)

The results of the post hoc test on the mean, median and SD of the QSM measures among the three groups (N+, N- and HC) are reported in Table 3.5.

ROI		N					
		N+ vs HC		N- vs HC		N+ vs N-	
		lh	rh	lh	rh	lh	rh
mean	wm-parietal-lobe	0,737	0,453	0,485	0,491	0,028	0,012
median	wm-frontal-lobe	/	1,000	/	0,103	/	0,118
	wm-parietal-lobe	/	0,636	/	0,430	/	0,017
SD	wm-frontal-lobe	/	1,000	/	0,070	/	0,036
	wm-temporal-lobe	/	0,179	/	0,032	/	1,000

Table 3.5 *Post hoc test on the mean, median and SD of QSM measures between the groups (N+, N-, HC).*

When significant, green and light blue highlight an increased and decreased value of the first group considered with respect to the second one, respectively.

3.2.7.1 Post hoc test correction for the age

For those variables which reached statistical significance in the post hoc test (N- and HC, N+ and N-), a non-parametric ANCOVA was applied using a Quade's test.

The group N- showed a statistically significant increase with respect to the group HC in the SD of QSM values in the right temporal lobe NAWM (p = .006).

There were no statistically significant differences comparing the mean of QSM values in the left and right parietal lobe NAWM, the median of QSM values in the right frontal lobe NAWM, the median of QSM values in the right parietal lobe NAWM and the SD of QSM values in the right frontal lobe NAWM, among the N+ and N- groups.

3.2.7.2 Binomial logistic regression

In addition to the approach explained in the previous paragraph, for those variables which reached statistical significance in the post hoc test, a binomial logistic regression was performed to predict the probability that a subject belongs to the group N- or HC, or the probability that a subject belongs to the group N+ or N-.

The model showed that the SD of QSM values in the right temporal lobe NAWM is statistically significant in predicting the belonging of a subject to the N- or HC group (p = .018), while the age is not (p = .340).

The models built to predict the belonging of a subject to the N+ or N- group showed that nor the neuroimaging variables considered (mean of QSM values in the left and right parietal lobe NAWM, median of QSM values in the right frontal lobe NAWM, median of QSM values in the right parietal lobe NAWM, SD of QSM values in the right frontal lobe NAWM), nor the age are statistically significant.

3.3 Neuroimaging measurements and clinical variables correlation

In the following paragraphs, the results of the correlation tests among the mean, median and SD of susceptibility measures and the clinical variables (disease duration, Aβ, P-Tau, T-tau, MMSE's score) are presented.

3.3.1 Correlations for the mean of the QSM values in the NAWM

The correlations computed for the mean of the susceptibility measures are described in Table 3.6.

QSM measurement		DURATION OF THE DISEASE	BA	TAU	PTAU	MMSE's score
NAWM_frontal_lh_QSM_mean	Corr.	0,225	-0,069	-0,091	-0,216	0,314
	Sig.	0,280	0,742	0,666	0,301	0,062
NAWM_cingulate_lh_QSM_mean	Corr.	0,307	-0,081	-0,064	-0,181	-0,019
	Sig.	0,135	0,701	0,762	0,386	0,911
NAWM_occipital_lh_QSM_mean	Corr.	-0,263	-0,229	0,177	-0,043	0,080
	Sig.	0,204	0,270	0,398	0,838	0,644
NAWM_temporal_lh_QSM_mean	Corr.	0,364	-0,016	-0,074	-0,020	0,060
	Sig.	0,073	0,939	0,726	0,923	0,728
NAWM_parietal_lh_QSM_mean	Corr.	0,209	-0,050	0,395	0,309	-0,009
	Sig.	0,317	0,812	0,050	0,132	0,958
NAWM_insula_lh_QSM_mean	Corr.	-0,071	-0,234	0,142	0,338	0,041
	Sig.	0,737	0,261	0,500	0,099	0,812
NAWM_frontal_rh_QSM_mean	Corr.	0,348	-0,164	0,181	0,169	0,232
	Sig.	0,088	0,434	0,387	0,418	0,174
NAWM_cingulate_rh_QSM_mean	Corr.	0,362	-0,085	-0,062	-0,082	0,041
	Sig.	0,075	0,685	0,767	0,697	0,814
NAWM_occipital_rh_QSM_mean	Corr.	-0,190	-0,229	0,000	-0,048	0,175
	Sig.	0,362	0,270	1,000	0,819	0,307
NAWM_temporal_rh_QSM_mean	Corr.	0,181	0,115	0,116	0,046	-0,036
	Sig.	0,388	0,583	0,580	0,828	0,836
NAWM_parietal_rh_QSM_mean	Corr.	0,171	-0,097	0,335	0,283	-0,055
	Sig.	0,413	0,645	0,102	0,170	0,749
NAWM_insula_rh_QSM_mean	Corr.	-0,117	-0,015	-0,093	0,056	-0,017
	Sig.	0,578	0,945	0,658	0,790	0,924

Table 3.6 *Correlations for the mean value of the susceptibility measures in the NAWM.*

3.3.2 Correlations for the median of the QSM values in the NAWM

The correlations computed for the median of the susceptibility measures are described in Table 3.7.

QSM measurement		DURATION OF THE DISEASE	BA	TAU	PTAU	MMSE's score
NAWM_frontal_lh_QSM_median	Corr.	0,279	0,028	0,042	-0,149	0,290
	Sig.	0,176	0,895	0,841	0,479	0,086
NAWM_cingulate_lh_QSM_median	Corr.	0,161	-0,131	-0,060	-0,192	0,000
	Sig.	0,443	0,533	0,776	0,359	0,999
NAWM_occipital_lh_QSM_median	Corr.	-0,246	-0,164	0,231	-0,044	0,073
	Sig.	0,236	0,434	0,267	0,835	0,673
NAWM_temporal_lh_QSM_median	Corr.	-0,039	0,062	0,115	0,017	0,051
	Sig.	0,852	0,770	0,585	0,937	0,768
NAWM_parietal_lh_QSM_median	Corr.	0,219	0,022	0,369	0,247	-0,020
	Sig.	0,293	0,916	0,069	0,235	0,908
NAWM_insula_lh_QSM_median	Corr.	0,029	0,128	-0,041	0,214	0,116
	Sig.	0,890	0,543	0,847	0,305	0,501
NAWM_frontal_rh_QSM_median	Corr.	0,395	-0,082	0,316	0,273	0,291
	Sig.	0,050	0,698	0,124	0,187	0,085
NAWM_cingulate_rh_QSM_median	Corr.	0,283	-0,034	-0,187	-0,169	0,087
	Sig.	0,170	0,872	0,371	0,421	0,614
NAWM_occipital_rh_QSM_median	Corr.	-0,280	-0,095	-0,173	-0,244	0,192
	Sig.	0,175	0,653	0,408	0,240	0,262
NAWM_temporal_rh_QSM_median	Corr.	-0,022	0,064	0,155	0,014	-0,041
	Sig.	0,916	0,762	0,458	0,948	0,813
NAWM_parietal_rh_QSM_median	Corr.	0,181	-0,096	0,354	0,304	-0,016
	Sig.	0,386	0,648	0,083	0,139	0,924
NAWM_insula_rh_QSM_median	Corr.	-0,072	0,019	0,005	0,089	0,106
	Sig.	0,732	0,927	0,980	0,671	0,540

Table 3.7 *Correlations for the median value of the susceptibility measures in the NAWM.*

3.3.3 Correlations for the SD of the QSM values in the NAWM

The correlations computed for the SD of the susceptibility measures are described in Table 3.8.

QSM measurement		DURATION OF THE DISEASE	BA	TAU	PTAU	MMSE's score
NAWM_frontal_lh_QSM_SD	Corr.	-0,184	-0,178	-0,292	**-0,426**	0,177
	Sig.	0,378	0,395	0,157	0,034	0,302
NAWM_cingulate_lh_QSM_SD	Corr.	0,351	-0,045	-0,052	-0,122	0,132
	Sig.	0,086	0,829	0,807	0,560	0,443
NAWM_occipital_lh_QSM_SD	Corr.	-0,389	0,358	-0,229	-0,194	0,186
	Sig.	0,055	0,079	0,270	0,352	0,277
NAWM_temporal_lh_QSM_SD	Corr.	0,093	-0,016	-0,225	-0,088	-0,001
	Sig.	0,658	0,939	0,280	0,675	0,996
NAWM_parietal_lh_QSM_SD	Corr.	-0,234	0,269	0,026	-0,079	0,133
	Sig.	0,261	0,193	0,901	0,706	0,440
NAWM_insula_lh_QSM_SD	Corr.	**0,529**	-0,037	-0,251	-0,095	-0,069
	Sig.	0,007	0,861	0,227	0,651	0,690
NAWM_frontal_rh_QSM_SD	Corr.	-0,115	0,123	**-0,418**	**-0,536**	0,032
	Sig.	0,584	0,558	0,037	0,006	0,854
NAWM_cingulate_rh_QSM_SD	Corr.	0,179	-0,177	-0,065	-0,142	0,122
	Sig.	0,392	0,398	0,756	0,498	0,477
NAWM_occipital_rh_QSM_SD	Corr.	**-0,440**	0,299	-0,041	-0,181	**0,403**
	Sig.	0,028	0,146	0,847	0,387	0,015
NAWM_temporal_rh_QSM_SD	Corr.	0,268	-0,176	-0,050	-0,031	-0,122
	Sig.	0,195	0,400	0,812	0,882	0,478
NAWM_parietal_rh_QSM_SD	Corr.	-0,124	0,293	-0,130	-0,223	0,130
	Sig.	0,554	0,155	0,536	0,283	0,449
NAWM_insula_rh_QSM_SD	Corr.	**0,534**	-0,054	-0,031	0,048	0,029
	Sig.	0,006	0,798	0,884	0,818	0,866

Table 3.8 *Correlations for the SD value of the susceptibility measures in the NAWM. Yellow and red highlight correlations significant at the 0.05 and 0.01 level, respectively.*

4. Discussion

Dementia is one of the major causes of disability and dependency among older people and there is no treatment or intervention that can be used to cure it or to modify its course [2].

The role of biochemical and imaging tools in the diagnosis of these diseases is assuming more and more importance. Indeed, the NIA-AA group updated the 2011 guidelines introducing the CSF biomarkers as the base of a new classification, that is the AT(N) classification, which is reproducible and independent from the neurologist clinical assessment and allows a common framework for defining and staging the disease, so that a standardized reporting of findings across the field is facilitated [5].

In addition, the new approach used for the characterization of the disorder combines information from clinical examinations, neuropsychological test (such as the MMSE) and imaging tools.

MRI is the most widely used neuroimaging technique to support the diagnosis of neurodegenerative disorders. It is exploited to study both volumetric and microstructural alterations of GM, but also to analyse changes in WM. These changes are usually called WM hyperintensities and are common incidental findings on brain images of older adults [13] and they are recognizable, often in greater extents, in AD patients (along with non-Alzheimer's dementias [14]).

However, more recent studies have demonstrated that WM damage spreads beyond the area of visible WMH, suggesting that the same pathogenic steps characterizing the development of the lesions are responsible also for the subtle "pre-visible" alterations in the surrounding normal-appearing white matter (NAWM) [38]. These studies evaluated mainly the alterations of the microstructure through the DTI technique. None of them measured the changes of susceptibility values in these regions, which appear normal on traditional MR imaging sequences.

In this thesis work QSM was employed due to its potential to evaluate subcortical NAWM damages in-vivo and in a non-invasive way in patients affected by neurodegenerative dementias.

We implemented a fully automatic method aimed at performing a whole-brain multi-metric characterization of subcortical WM alterations.

The neuroimaging measurements that were extracted from the ROIs were the mean, median and SD of susceptibility values in each of the 6 lobes (frontal, cingulate, occipital, temporal, parietal, insula) considered for each hemisphere. These measures were also combined with clinical information regarding the duration of the disease and the MMSE's score. In the following paragraphs the most significant results from a clinical point of view will be discussed and assessed.

For what concerns the neuroimaging measurements group comparisons, more statistical evidence was found when we stratified the patients according to the CSF biomarkers-based classifications with respect to the ND vs HC group classification. This suggests that a biological classification, determined using the biomarkers, allows the stratification of the subjects with different susceptibility characteristics, caused by the pathologic processes typical of the neurodegenerative diseases, such as iron overload and demyelination.
Particularly, between the three CSF biomarkers-based classifications, the one based on the value of the T-tau (N) demonstrated the largest amount of statistically significant comparisons among the groups.

Considering that in healthy aging accumulation of iron occurs in several brain regions and cell types [54], and that our results of the age comparison among groups highlighted a trend, age-related accumulation of iron may have an influence on our measure of susceptibility.
However, the SD of QSM values in the right temporal lobe NAWM remained significant both after the correction for age and in the prediction model created. This suggests that our measure might be a predictor of the N-based group to which a subject belongs to, independently from the age.
The fact that some alterations of susceptibility occur mainly in one lobe may be related to the accumulation of iron in specific brain regions which is greater than that reported in

healthy aging in many neurodegenerative diseases and is often associated with oxidative stress and cellular damage [54].

Moreover, different subjects in our group of study were diagnosed with frontotemporal dementia, which principally affects the frontal and temporal lobes. The same results are not obtained for the frontal lobe probably due to the streaking artefact present in some susceptibility maps, caused by the large susceptibility difference at the tissue and air interface that characterizes this region.

It is also known that temporal lobe structures, such as the hippocampal formation, parahippocampal gyrus, and entorhinal cortex, tend to degenerate early [52]. *Huang et al.* [52] found evidence for functionally relevant microstructural changes in the NAWM of patients with AD and MCI. These changes were present in brain regions serving higher cortical functions, but not in regions serving primary functions, and are consistent with a hypothesized loss of axonal processes in the temporal lobe. This apparent regional gradient in white matter changes closely parallels the known distribution of regional neuropathology in AD [53].

As regards the CSF biomarkers, it has been showed that, differently from the Aβ biomarker which is not associated with the disease progression, very high levels of both P-tau and T-tau may be associated with the severity of the disease [1].

Nevertheless, in light of the limited correlations between these biomarkers and the duration of the disease with our neuroimaging measures, we can affirm that the QSM measures do not follow the progress of the pathology.

In this respect, it could be interesting to verify if our measures might be used as a biomarker for the identification of pre-symptomatic individuals at higher risk of developing a type of dementia. This would be a fundamental element to “prevent the preventable”.

Our study showed how the SD value of susceptibility measures in the NAWM might be used as a support for the characterization of the pathological profile of a subject in a completely non-invasive way. Therefore, these measurements may be associated with the lumbar puncture providing additional information without introducing increased costs

in the examination: one of the main advantage of the MRI is that it is an imaging tool able to provide multiple types of data with just one acquisition.

Moreover, a relevant aspect of this work is the automatic segmentation of both the subcortical WM and of the WMHs, which overcomes the dependence of the selected regions to the ability of the operator and achieves the reproducibility which was not available in hand-made regions of interest.

However, some limitations need to be acknowledged.

First, in order to have more meaningful results, an enlargement of the group of study is required. The ND group is composed by a limited number of patients and, given the large variety of diagnoses that characterize them, a more suitable classification is needed to better differentiate the different disorders included in the group. For example, if the number of subjects increases, it will be possible to subdivide them according to all the 8 possible profiles given by the different combinations of the three CSF biomarkers: (1) normal [A−T−(N−)]; (2) AD-continuum ([A+T−(N−)], [A+T+(N−)], [A+T+(N+)] and [A+T−(N+)]); and (3) non-AD pathologic change (non-AD) ([A−T+(N−)], [A−T−(N+)] and [A−T+(N+)]) [5].

Then, another limitation is related to the QSM technique, which assumes that susceptibility is isotropic, even if recent studies found that susceptibility of brain WM is anisotropic. This approximation may be handled exploiting a novel application, called *Susceptibility Tensor Imaging* (STI). A susceptibility tensor imaging was proposed to measure and quantify this phenomenon, since this technique relies on the measurement of frequency offsets at different orientations with respect to the main magnetic field. Therefore, the orientation dependence of susceptibility is characterized by a tensor.

Another future improvement could be that of putting together the information coming from QSM and DTI, given the conjoint potential offered by these advanced MRI techniques.

Finally, in view of the amount of neuroimaging measurements and clinical variables available, another development may be given by the usage of machine learning algorithms to create more accurate predictive models, that put together evidence coming from the CSF biomarkers, that represent the neurologic point of view, from the MMSE or

other tests, that represent the neuropsychological point of view, and the neuroimaging measurements.

The automaticity of the pipeline facilitates the validation of the method on larger groups of patients, and that might represent an additional tool for patient stratification in clinical trials and then for neurologists in their clinical practice.

5. Conclusions

For the first time, a fully automatic neuroimaging pipeline was developed and applied for the quantification of susceptibility in the NAWM, in order to highlight anomalies in patients suffering from neurodegenerative dementia classified according to the CSF-biomarkers.

The study highlighted that QSM measures are sensitive to tissue characteristics in the neurodegenerative dementia groups, especially between with (N+) and without (N-) tau-defined neurodegeneration. Particularly, the SD of QSM values in the temporal lobe NAWM showed the strongest significance, being a predictor independent from the age.
In addition, given the link between the classifications based on the CSF biomarkers and the values of susceptibility measures, in future QSM might be exploited as an additional non-invasive tool for patient stratification in clinical trials.

The strengths of this work are related to the automaticity and non-invasiveness of the techniques applied, both in the segmentation of the lesions and the generation of the susceptibility maps.

The current thesis work could be further improved with the application of different MRI modalities and machine learning algorithms to enlarge the measurements pool and test for more complex classification and prediction models.

References

[1] Sancesario GM, Bernardini S. *Diagnosis of neurodegenerative dementia: where do we stand, now?* Ann Transl Med. 2018 Sep;6(17):340.

[2] https://www.who.int/

[3] Knopman DS, Boeve BF, Petersen RC. *Essentials of the proper diagnoses of mild cognitive impairment, dementia, and major subtypes of dementia.* Mayo Clin Proc. 2003 Oct;78(10):1290-308.

[4] Geschwind MD, Shu H, Haman A, Sejvar JJ, Miller BL. *Rapidly progressive dementia.* Ann Neurol. 2008 Jul;64(1):97-108.

[5] Jack CR Jr, Bennett DA, Blennow K, Carrillo MC, Dunn B, Haeberlein SB, Holtzman DM, Jagust W, Jessen F, Karlawish J, Liu E, Molinuevo JL, Montine T, Phelps C, Rankin KP, Rowe CC, Scheltens P, Siemers E, Snyder HM, Sperling R; Contributors. *NIA-AA Research Framework: Toward a biological definition of Alzheimer's disease.* Alzheimers Dement. 2018 Apr;14(4):535-562.

[6] McKhann GM, Knopman DS, Chertkow H, Hyman BT, Jack CR Jr, Kawas CH, Klunk WE, Koroshetz WJ, Manly JJ, Mayeux R, Mohs RC, Morris JC, Rossor MN, Scheltens P, Carrillo MC, Thies B, Weintraub S, Phelps CH. *The diagnosis of dementia due to Alzheimer's disease: recommendations from the National Institute on Aging-Alzheimer's Association workgroups on diagnostic guidelines for Alzheimer's disease.* Alzheimers Dement. 2011 May;7(3):263-9.

[7] Albert MS, DeKosky ST, Dickson D, Dubois B, Feldman HH, Fox NC, Gamst A, Holtzman DM, Jagust WJ, Petersen RC, Snyder PJ, Carrillo MC, Thies B, Phelps CH. *The diagnosis of mild cognitive impairment due to Alzheimer's disease: recommendations from*

the National Institute on Aging-Alzheimer's Association workgroups on diagnostic guidelines for Alzheimer's disease. Alzheimers Dement. 2011 May;7(3):270-9.

[8] Sperling RA, Aisen PS, Beckett LA, Bennett DA, Craft S, Fagan AM, Iwatsubo T, Jack CR Jr, Kaye J, Montine TJ, Park DC, Reiman EM, Rowe CC, Siemers E, Stern Y, Yaffe K, Carrillo MC, Thies B, Morrison-Bogorad M, Wagster MV, Phelps CH. *Toward defining the preclinical stages of Alzheimer's disease: recommendations from the National Institute on Aging-Alzheimer's Association workgroups on diagnostic guidelines for Alzheimer's disease.* Alzheimers Dement. 2011 May;7(3):280-92.

[9] Rajan KB, Wilson RS, Weuve J, Barnes LL, Evans DA. *Cognitive impairment 18 years before clinical diagnosis of Alzheimer disease dementia.* Neurology. 2015 Sep 8;85(10):898-904.

[10] Rita Khoury, Elias Ghossoub. *Diagnostic biomarkers of Alzheimer's disease: A state-of-the-art review*. Biomarkers in Neuropsychiatry. 2019;1(November):100005.

[11] Pini L, Pievani M, Bocchetta M, Altomare D, Bosco P, Cavedo E, Galluzzi S, Marizzoni M, Frisoni GB. *Brain atrophy in Alzheimer's Disease and aging.* Ageing Res Rev. 2016 Sep;30:25-48.

[12] Nasrabady SE, Rizvi B, Goldman JE, Brickman AM. *White matter changes in Alzheimer's disease: a focus on myelin and oligodendrocytes.* Acta Neuropathol Commun. 2018 Mar 2;6(1):22.

[13] Lindemer ER, Greve DN, Fischl BR, Augustinack JC, Salat DH. *Regional staging of white matter signal abnormalities in aging and Alzheimer's disease.* Neuroimage Clin. 2017 Jan 23;14:156-165.

[14] Filippi M, Agosta F. *MRI of non-Alzheimer's dementia: current and emerging knowledge.* Curr Opin Neurol. 2018 Aug;31(4):405-414.

[15] Fazekas F, Kleinert R, Offenbacher H, Schmidt R, Kleinert G, Payer F, Radner H, Lechner H. *Pathologic correlates of incidental MRI white matter signal hyperintensities.* Neurology. 1993 Sep;43(9):1683-9.

[16] Brown WR, Thore CR. *Review: cerebral microvascular pathology in ageing and neurodegeneration*. Neuropathol Appl Neurobiol. 2011 Feb;37(1):56-74.

[17] McAleese KE, Walker L, Graham S, Moya ELJ, Johnson M, Erskine D, Colloby SJ, Dey M, Martin-Ruiz C, Taylor JP, Thomas AJ, McKeith IG, De Carli C, Attems J. *Parietal white matter lesions in Alzheimer's disease are associated with cortical neurodegenerative pathology, but not with small vessel disease*. Acta Neuropathol. 2017 Sep;134(3):459-473.

[18] Daglas M, Adlard PA. *The Involvement of Iron in Traumatic Brain Injury and Neurodegenerative Disease.* Front Neurosci. 2018 Dec 20;12:981.

[19] Ke Y, Qian ZM. *Brain iron metabolism: neurobiology and neurochemistry.* Prog Neurobiol. 2007 Oct;83(3):149-73.

[20] Urrutia PJ, Mena NP, Núñez MT. *The interplay between iron accumulation, mitochondrial dysfunction, and inflammation during the execution step of neurodegenerative disorders.* Front Pharmacol. 2014 Mar 10;5:38.

[21] Liu JL, Fan YG, Yang ZS, Wang ZY, Guo C. *Iron and Alzheimer's Disease: From Pathogenesis to Therapeutic Implications.* Front Neurosci. 2018 Sep 10;12:632.

[22] Wong BX, Tsatsanis A, Lim LQ, Adlard PA, Bush AI, Duce JA. *β-Amyloid precursor protein does not possess ferroxidase activity but does stabilize the cell surface ferrous iron exporter ferroportin.* PLoS One. 2014 Dec 2;9(12):e114174.

[23] Belaidi AA, Bush AI. *Iron neurochemistry in Alzheimer's disease and Parkinson's disease: targets for therapeutics.* J Neurochem. 2016 Oct;139 Suppl 1:179-197.

[24] Liu C, Wei H, Gong NJ, Cronin M, Dibb R, Decker K. *Quantitative Susceptibility Mapping: Contrast Mechanisms and Clinical Applications.* Tomography. 2015 Sep;1(1):3-17.

[25] Liu C, Li W, Tong KA, Yeom KW, Kuzminski S. *Susceptibility-weighted imaging and quantitative susceptibility mapping in the brain.* J Magn Reson Imaging. 2015 Jul;42(1):23-41.

[26] Ruetten PPR, Gillard JH, Graves MJ. *Introduction to Quantitative Susceptibility Mapping and Susceptibility Weighted Imaging.* Br J Radiol. 2019 Sep;92(1101):20181016.

[27] Vinayagamani S, Sheelakumari R, Sabarish S, Senthilvelan S, Ros R, Thomas B, Kesavadas C. *Quantitative Susceptibility Mapping: Technical Considerations and Clinical Applications in Neuroimaging.* J Magn Reson Imaging. 2020 Jan 17.

[28] Haacke EM, Xu Y, Cheng YC, Reichenbach JR. *Susceptibility weighted imaging (SWI).* Magn Reson Med. 2004 Sep;52(3):612-8.

[29] Wang Y, Liu T. *Quantitative susceptibility mapping (QSM): Decoding MRI data for a tissue magnetic biomarker.* Magn Reson Med. 2015 Jan;73(1):82-101.

[30] Li W, Wu B, Batrachenko A, Bancroft-Wu V, Morey RA, Shashi V, Langkammer C, De Bellis MD, Ropele S, Song AW, Liu C. *Differential developmental trajectories of magnetic susceptibility in human brain gray and white matter over the lifespan.* Hum Brain Mapp. 2014 Jun;35(6):2698-713.

[31] Paul Schmidt. *Bayesian inference for structured additive regression models for large-scale problems with applications to medical imaging.* PhD thesis, Ludwig Maximilians - Universität München, Januar 2017.
URL http://nbn-resolving.de/urn:nbn:de:bvb:19-203731.

[32] Li W, Avram AV, Wu B, Xiao X, Liu C. *Integrated Laplacian-based phase unwrapping and background phase removal for quantitative susceptibility mapping.* NMR Biomed. 2014 Feb;27(2):219-27.

[33] Wei Li, Chunlei Liu, *STI Suite User Manual.*

[34] Wei H, Dibb R, Zhou Y, Sun Y, Xu J, Wang N, Liu C. *Streaking artifact reduction for quantitative susceptibility mapping of sources with large dynamic range.* NMR Biomed. 2015 Oct;28(10):1294-303.

[35] http://surfer.nmr.mgh.harvard.edu/

[36] Desikan RS, Ségonne F, Fischl B, Quinn BT, Dickerson BC, Blacker D, Buckner RL, Dale AM, Maguire RP, Hyman BT, Albert MS, Killiany RJ. *An automated labeling system for subdividing the human cerebral cortex on MRI scans into gyral based regions of interest.* Neuroimage. 2006 Jul 1;31(3):968-80.

[37] Salat DH, Greve DN, Pacheco JL, Quinn BT, Helmer KG, Buckner RL, Fischl B. *Regional white matter volume differences in nondemented aging and Alzheimer's disease.* Neuroimage. 2009 Feb 15;44(4):1247-58.

[38] Muñoz Maniega S, Chappell FM, Valdés Hernández MC, Armitage PA, Makin SD, Heye AK, Thrippleton MJ, Sakka E, Shuler K, Dennis MS, Wardlaw JM. *Integrity of normal-appearing white matter: Influence of age, visible lesion burden and hypertension in patients with small-vessel disease.* J Cereb Blood Flow Metab. 2017 Feb;37(2):644-656.

[39] Vernooij MW, de Groot M, van der Lugt A, Ikram MA, Krestin GP, Hofman A, Niessen WJ, Breteler MM. *White matter atrophy and lesion formation explain the loss of structural integrity of white matter in aging.* Neuroimage. 2008 Nov 15;43(3):470-7.

[40] Park M, Moon Y, Han SH, Kim HK, Moon WJ. *Myelin loss in white matter hyperintensities and normal-appearing white matter of cognitively impaired patients: a*

quantitative synthetic magnetic resonance imaging study. Eur Radiol. 2019 Sep;29(9):4914-4921.

[41] Carandini T, Arighi A, Sacchi L, Fumagalli GG, Pietroboni AM, Ghezzi L, Colombi A, Scarioni M, Fenoglio C, De Riz MA, Marotta G, Scarpini E, Galimberti D. *Testing the 2018 NIA-AA research framework in a retrospective large cohort of patients with cognitive impairment: from biological biomarkers to clinical syndromes.* Alzheimers Res Ther. 2019 Oct 15;11(1):84.

[42] McKhann G, Drachman D, Folstein M, Katzman R, Price D, Stadlan EM. *Clinical diagnosis of Alzheimer's disease: report of the NINCDS-ADRDA Work Group under the auspices of Department of Health and Human Services Task Force on Alzheimer's Disease.* Neurology. 1984 Jul;34(7):939-44.

[43] Dubois B, Feldman HH, Jacova C, Dekosky ST, Barberger-Gateau P, Cummings J, Delacourte A, Galasko D, Gauthier S, Jicha G, Meguro K, O'brien J, Pasquier F, Robert P, Rossor M, Salloway S, Stern Y, Visser PJ, Scheltens P. *Research criteria for the diagnosis of Alzheimer's disease: revising the NINCDS-ADRDA criteria.* Lancet Neurol. 2007 Aug;6(8):734-46.

[44] Dubois B, Feldman HH, Jacova C, Hampel H, Molinuevo JL, Blennow K, DeKosky ST, Gauthier S, Selkoe D, Bateman R, Cappa S, Crutch S, Engelborghs S, Frisoni GB, Fox NC, Galasko D, Habert MO, Jicha GA, Nordberg A, Pasquier F, Rabinovici G, Robert P, Rowe C, Salloway S, Sarazin M, Epelbaum S, de Souza LC, Vellas B, Visser PJ, Schneider L, Stern Y, Scheltens P, Cummings JL. *Advancing research diagnostic criteria for Alzheimer's disease: the IWG-2 criteria.* Lancet Neurol. 2014 Jun;13(6):614-29.

[45] Gorno-Tempini ML, Hillis AE, Weintraub S, Kertesz A, Mendez M, Cappa SF, Ogar JM, Rohrer JD, Black S, Boeve BF, Manes F, Dronkers NF, Vandenberghe R, Rascovsky K, Patterson K, Miller BL, Knopman DS, Hodges JR, Mesulam MM, Grossman M. *Classification of primary progressive aphasia and its variants.* Neurology. 2011 Mar 15;76(11):1006-14.

[46] Rascovsky K, Hodges JR, Knopman D, Mendez MF, Kramer JH, Neuhaus J, van Swieten JC, Seelaar H, Dopper EG, Onyike CU, Hillis AE, Josephs KA, Boeve BF, Kertesz A, Seeley WW, Rankin KP, Johnson JK, Gorno-Tempini ML, Rosen H, Prioleau-Latham CE, Lee A, Kipps CM, Lillo P, Piguet O, Rohrer JD, Rossor MN, Warren JD, Fox NC, Galasko D, Salmon DP, Black SE, Mesulam M, Weintraub S, Dickerson BC, Diehl-Schmid J, Pasquier F, Deramecourt V, Lebert F, Pijnenburg Y, Chow TW, Manes F, Grafman J, Cappa SF, Freedman M, Grossman M, Miller BL. *Sensitivity of revised diagnostic criteria for the behavioural variant of frontotemporal dementia.* Brain. 2011 Sep;134(Pt 9):2456-77.

[47] McKeith IG, Boeve BF, Dickson DW, Halliday G, Taylor JP, Weintraub D, Aarsland D, Galvin J, Attems J, Ballard CG, Bayston A, Beach TG, Blanc F, Bohnen N, Bonanni L, Bras J, Brundin P, Burn D, Chen-Plotkin A, Duda JE, El-Agnaf O, Feldman H, Ferman TJ, Ffytche D, Fujishiro H, Galasko D, Goldman JG, Gomperts SN, Graff-Radford NR, Honig LS, Iranzo A, Kantarci K, Kaufer D, Kukull W, Lee VMY, Leverenz JB, Lewis S, Lippa C, Lunde A, Masellis M, Masliah E, McLean P, Mollenhauer B, Montine TJ, Moreno E, Mori E, Murray M, O'Brien JT, Orimo S, Postuma RB, Ramaswamy S, Ross OA, Salmon DP, Singleton A, Taylor A, Thomas A, Tiraboschi P, Toledo JB, Trojanowski JQ, Tsuang D, Walker Z, Yamada M, Kosaka K. *Diagnosis and management of dementia with Lewy bodies: Fourth consensus report of the DLB Consortium.* Neurology. 2017 Jul 4;89(1):88-100.

[48] Armstrong MJ, Litvan I, Lang AE, Bak TH, Bhatia KP, Borroni B, Boxer AL, Dickson DW, Grossman M, Hallett M, Josephs KA, Kertesz A, Lee SE, Miller BL, Reich SG, Riley DE, Tolosa E, Tröster AI, Vidailhet M, Weiner WJ. *Criteria for the diagnosis of corticobasal degeneration.* Neurology. 2013 Jan 29;80(5):496-503.

[49] Postuma RB, Berg D, Stern M, Poewe W, Olanow CW, Oertel W, Obeso J, Marek K, Litvan I, Lang AE, Halliday G, Goetz CG, Gasser T, Dubois B, Chan P, Bloem BR, Adler CH, Deuschl G. *MDS clinical diagnostic criteria for Parkinson's disease.* Mov Disord. 2015 Oct;30(12):1591-601.

[50] Litvan I, Agid Y, Calne D, Campbell G, Dubois B, Duvoisin RC, Goetz CG, Golbe LI, Grafman J, Growdon JH, Hallett M, Jankovic J, Quinn NP, Tolosa E, Zee DS. *Clinical research criteria for the diagnosis of progressive supranuclear palsy (Steele-Richardson-Olszewski syndrome): report of the NINDS-SPSP international workshop.* Neurology. 1996 Jul;47(1):1-9.

[51] Gorelick PB, Scuteri A, Black SE, Decarli C, Greenberg SM, Iadecola C, Launer LJ, Laurent S, Lopez OL, Nyenhuis D, Petersen RC, Schneider JA, Tzourio C, Arnett DK, Bennett DA, Chui HC, Higashida RT, Lindquist R, Nilsson PM, Roman GC, Sellke FW, Seshadri S; American Heart Association Stroke Council, Council on Epidemiology and Prevention, Council on Cardiovascular Nursing, Council on Cardiovascular Radiology and Intervention, and Council on Cardiovascular Surgery and Anesthesia. *Vascular contributions to cognitive impairment and dementia: a statement for healthcare professionals from the american heart association/american stroke association.* Stroke. 2011 Sep;42(9):2672-713.

[52] Huang J, Friedland RP, Auchus AP. *Diffusion tensor imaging of normal-appearing white matter in mild cognitive impairment and early Alzheimer disease: preliminary evidence of axonal degeneration in the temporal lobe.* AJNR Am J Neuroradiol. 2007 Nov-Dec;28(10):1943-8.

[53] Braak E, Griffing K, Arai K, Bohl J, Bratzke H, Braak H. *Neuropathology of Alzheimer's disease: what is new since A. Alzheimer?* Eur Arch Psychiatry Clin Neurosci. 1999;249 Suppl 3:14-22.

[54] Ward RJ, Zucca FA, Duyn JH, Crichton RR, Zecca L. *The role of iron in brain ageing and neurodegenerative disorders.* Lancet Neurol. 2014 Oct;13(10):1045-60.